HHS Public Access

Author manuscript

Cell Rep. Author manuscript; available in PMC 2024 May 09.

Published in final edited form as:

Cell Rep. 2024 April 23; 43(4): 114009. doi:10.1016/j.celrep.2024.114009.

Distinct subpopulations of ventral pallidal cholinergic projection neurons encode valence of olfactory stimuli

Ronald Kim[1], **Mala R. Ananth**[2], **Niraj S. Desai**[2], **Lorna W. Role**[2,3,*], **David A. Talmage**[1,3,4,*]

[1]Genetics of Neuronal Signaling Section, National Institute of Neurological Disorders and Stroke, National Institutes of Health, Bethesda, MD 20892, USA

[2]Circuits, Synapses and Molecular Signaling Section, National Institute of Neurological Disorders and Stroke, National Institutes of Health, Bethesda, MD 20892, USA

[3]These authors contributed equally

[4]Lead contact

SUMMARY

To better understand the function of cholinergic projection neurons in the ventral pallidum (VP), we examined behavioral responses to appetitive (APP) and aversive (AV) odors that elicited approach or avoidance, respectively. Exposure to each odor increased cFos expression and calcium signaling in VP cholinergic neurons. Activity and Cre-dependent viral vectors selectively labeled VP cholinergic neurons that were activated and reactivated in response to either APP or AV odors, but not both, identifying two non-overlapping populations of VP cholinergic neurons differentially activated by the valence of olfactory stimuli. These two subpopulations showed differences in electrophysiological properties, morphology, and projections to the basolateral amygdala. Although VP neurons are engaged in both approach and avoidance behavioral responses, cholinergic signaling is only required for approach behavior. Thus, two distinct subpopulations of VP cholinergic neurons differentially encode valence of olfactory stimuli and play distinct roles in approach and avoidance behaviors.

Graphical abstract

*Correspondence: lorna.role@nih.gov (L.W.R.), david.talmage@nih.gov (D.A.T.).

AUTHOR CONTRIBUTIONS

R.K., M.A., L.W.R., and D.A.T. designed the experiments. R.K., M.A., and N.S.D. performed the experiments and analyzed the data. R.K., L.W.R., and D.A.T. wrote the article.

SUPPLEMENTAL INFORMATION

Supplemental information can be found online at https://doi.org/10.1016/j.celrep.2024.114009.

DECLARATION OF INTERESTS

The authors declare no competing interests.

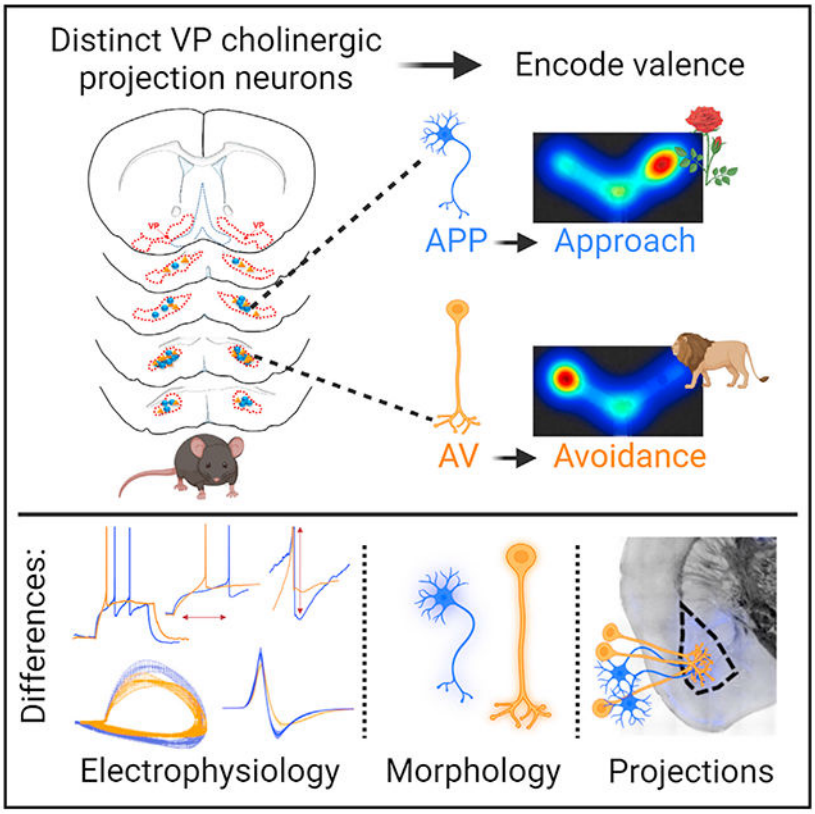

In brief

Kim et al. identify two distinct subpopulations of VP cholinergic projection neurons activated by an appetitive vs. aversive odor. These two subpopulations display different properties, which indicate differential integration of each subpopulation into neural circuits. These results demonstrate functional heterogeneity of VP cholinergic neurons.

INTRODUCTION

Proper decision making is critical for survival in a dynamic environment with both appetitive (APP) and aversive (AV) stimuli. This entails motivation to approach and retrieve rewarding stimuli as well as motivation to avoid harmful stimuli. The first step in any behavior is the ability to properly encode valence.[1] The valence of the stimulus (either positive or negative) then directs the animal toward an appropriate behavioral output. Generally, animals demonstrate approach behavior toward positive valence stimuli while avoiding negative valence stimuli.[1–3] Misattributions of valence can lead to maladaptive behaviors. Furthermore, prolonged improper valence encoding can lead to the development of psychiatric diseases such as drug addiction and depression.[4,5] Examining the brain regions and neural circuits that underlie proper valence encoding is essential to understanding the mechanisms underlying motivated behaviors.

The ventral pallidum (VP) is involved in mediating motivated behaviors.[6–10] The VP coordinates limbic inputs and regulates motivated behaviors in response to these inputs.[8,11] The VP has been implicated in a variety of neuropsychiatric disorders that are characterized by motivational imbalance, including drug addiction, depression, stress, and anxiety.[12–16] The VP modulates motivation via the activity of multiple different cell types. γ-aminobutyric acid (GABA) projection neurons in the VP increase motivation to receive a rewarding stimulus.[9,17,18] For example, optogenetic stimulation of VP GABA neurons makes a stimulus appear more rewarding and can drive reinforcement behavior.[9,17] In contrast, stimulation of glutamatergic projection neurons in the VP enhances aversive responses, leading to avoidance.[9,17]

In addition to GABA and glutamate neurons, the VP includes a small population of cholinergic neurons that project out of the VP to targets that include the basolateral amygdala (BLA), medial prefrontal cortex (mPFC), and thalamus.[8,17,19] The functional significance of VP cholinergic projection neurons is unclear. Stephenson-Jones and colleagues identified a cluster of VP neurons, described as type I neurons, whose firing patterns differed from that of either VP GABAergic or glutamatergic neurons.[9] Unlike VP GABA or glutamatergic neurons, these neurons responded to both aversive and rewarding stimuli.[9] These type I VP neurons were hypothesized to be salience-encoding cholinergic neurons, since their activity patterns resemble those of cholinergic neurons in other parts of the basal forebrain that respond to both reward and punishment.[20]

Despite the known presence of cholinergic projection neurons in the VP, the functional significance of these neurons remains unknown. Although VP GABA and glutamate neurons have a unique role in processing rewarding vs. aversive behaviors, the role of VP cholinergic neurons in approach vs. aversive behaviors is unknown. Accordingly, we utilized activity- and Cre-dependent viral vectors to permanently label activated VP cholinergic neurons in distinct behavioral contexts. Here, we demonstrate that the VP includes two non-overlapping subpopulations of cholinergic neurons: one activated in response to APP odors and a second, distinct subpopulation activated in response to AV odors. These two subpopulations of VP cholinergic projection neurons are spatially intermingled within the VP but are differentiated from one another in several key characteristics including electro-physiological properties, overall neuronal morphology, and projections to downstream brain regions. Importantly, although VP cholinergic neurons are engaged in APP and AV behavioral responses, VP cholinergic signaling is required for approach behavior, whereas AV behaviors are not exclusively dependent on VP cholinergic signaling.

RESULTS

APP and AV odors elicit innate behavioral responses

To examine whether VP cholinergic neurons were engaged in APP and/or AV behaviors, we first measured behavioral responses to an APP odor (2-phenylethanol) and an AV odor (predator odor, mountain lion urine) (Figure 1A). In a preference test between saline (SAL) and the APP odor, mice spent significantly more time in the arm with the APP odor ($t(16) = -5.7$, $p < 0.001$; Figures 1B and 1C), indicating approach to the APP odor. In contrast, in a preference test between SAL and the AV odor, mice spent significantly more time in the arm

with SAL ($t(14) = -5.06$, $p < 0.001$; Figures 1B and 1C), indicating avoidance of the AV odor. Neither the APP nor the AV odor affected total distance traveled or velocity (Figures S1A and S1B). We did not find any sex differences in approach or avoidance behavior in response to odor exposure (Figures S1C and S1D).

Approach and avoidance behaviors engage VP cholinergic neurons

To test whether immediate-early gene expression (cFos) was increased in VP cholinergic neurons following odor exposure, mice were euthanized ~45 min following the odor preference test (Figures 1A–1C), and fixed tissue slices containing the VP were stained with antibodies recognizing choline acetyltransferase (ChAT; cholinergic neurons) and cFos (as a marker of neuronal activation) (Figures 1D and 1E). The total number of $cFos^+$ cells in the VP significantly increased following exposure to either odor ($F(2, 64) = 12.79$, $p < 0.001$; pairwise comparisons: APP vs. SAL [$t = 4.29$, $p < 0.001$], AV vs. SAL [$t = 4.64$, $p < 0.001$]; Figure 1F, right). Cholinergic neurons were activated following exposure to either odor (number of co-localized ChAT and $cFos^+$ neurons [Figure 1G, left]: $F(2, 64) = 4.19$, $p < 0.05$; pairwise comparison: APP vs. SAL [$t = 2.77$, $p < 0.05$], AV vs. SAL [$t = 2.26$, $p < 0.05$]; percentage of ChAT neurons that were $cFos^+$ after odor exposure [Figure 1G, right]: $F(2, 64) = 4.35$, $p < 0.05$; pairwise comparisons: APP vs. SAL [$t = 2.63$, $p < 0.05$], AV vs. SAL [$t = 2.59$, $p < 0.05$]). The number of cholinergic neurons identified was equivalent between groups (ChAT counts; Figure 1F, left).

VP cholinergic neurons display time-locked increases in calcium activity in direct response to each odor

To examine the activity of VP cholinergic neurons in direct response to each odor, we used Cre-dependent GCaMP6f and *in vivo* fiber photometry to measure calcium responses of VP cholinergic neurons during timed odor delivery. Both the APP odor (Figures 1I, 1K, and 1M) and the AV odor (Figures 1J, 1L, and 1N) increased calcium activity of VP cholinergic neurons during the 10-s delivery of each odor. The area under the curve (AUC) was significantly increased during each APP odor delivery ($F(4, 34) = 14.28$, $p < 0.001$, Figure 1K; pairwise comparisons: APP 1 vs. pre-odor [$t = 6.35$, $p < 0.001$], APP 1 vs. post-odor [$t = 5.66$, $p < 0.001$], APP 2 vs. pre-odor [$t = 3.02$, $p < 0.05$], APP 3 vs. pre-odor [$t = 4.74$, $p < 0.001$], APP 3 vs. post-odor [$t = 4.04$, $p < 0.05$]). Likewise, the integrated Ca^{2+} signal (AUC), was significantly increased following each AV odor delivery ($F(4, 34) = 12.34$, $p < 0.001$, Figure 1L; pairwise comparisons: AV 1 vs. pre-odor [$t = 5.78$, $p < 0.001$], AV 1 vs. post-odor [$t = 5.15$, $p < 0.001$], AV 2 vs. pre-odor [$t = 4.16$, $p < 0.05$], AV 2 vs. post-odor [$t = 3.53$, $p < 0.05$], AV 3 vs. pre-odor [$t = 3.81$, $p < 0.05$], AV 3 vs. post-odor [$t = 3.19$, $p < 0.05$]). The maximum Z-score $\times F/F$ was significantly increased during the first APP odor ($F(4, 34) = 4.4$, $p < 0.05$; $t = 3.69$, $p < 0.05$; Figure 1M) and first AV odor ($F(4, 34) = 5.19$, $p < 0.05$; $t = 3.90$, $p < 0.05$; Figure 1N). These results corroborate our immunohistochemistry (IHC) results and confirm that both APP and AV odors directly engage VP cholinergic neurons.

Silencing VP cholinergic neurons not only abolishes but reverses approach behavior to active avoidance of the APP odor

To test the requisite participation of VP cholinergic neurons in approach or avoidance behaviors, we used a Cre-dependent inhibitory designer receptor exclusively activated by designer drugs (DREADD) to silence cholinergic neurons in the VP (Figure 2). Previous experiments have demonstrated the efficacy of DREADDs for altering the activity of cholinergic neurons and for influencing behavior.[16,21–24] In a preference test with the APP odor, mice in the sham group (eGFP only + clozapine) exhibited approach to the APP odor (Figures 2B [left] and 2C). In contrast, hM4Di inhibition of VP cholinergic neurons abolished this effect, and mice spent significantly more time in the SAL arm than in the arm with the APP odor ($t(8) = 4.21$, $p < 0.05$; Figures 2B [right] and 2C), consistent with active avoidance of the APP odor. Thus, VP cholinergic signaling not only is required for approach behavior, but inhibition of cholinergic neurons in the VP leads to active avoidance of the APP odor.

In contrast to the dramatic effects of hM4Di inhibition of VP cholinergic neurons on the reversal of approach to the APP odor, the behavioral response toward the AV odor was resistant to VP cholinergic inhibition. In a preference test with the AV odor, mice in the sham group exhibited avoidance of the AV odor (Figures 2D [left] and 2E). Mice with hM4Di inhibition of VP cholinergic neurons also displayed avoidance of the AV odor (Figures 2D [right] and 2E). These results indicate that inhibition of cholinergic signaling in the VP was not sufficient to alter avoidance of the AV odor. These results were not due to any hM4Di-induced changes in behavior, as mice in both groups displayed comparable locomotor activity (Figures S3A–S3D). Furthermore, mice with hM4Di inhibition of VP cholinergic neurons displayed equal time spent in each arm during a preference test with SAL in both arms of the Y-maze (Figures S3E and S3F), further indicating that hM4Di inhibition of cholinergic neurons did not induce general changes in behavior.

Distinct and non-overlapping subpopulations of VP cholinergic neurons are activated in response to APP vs. AV odors

Exposure to either odor led to cFos expression in equivalent numbers (~20%) of VP cholinergic neurons (Figures 1D–1G) and resulted in a similar increase in calcium activity (Figures 1H–1N). To determine whether the same or distinct subpopulations of VP cholinergic neurons were activated in response to each odor, we injected the VP of ChAT-Cre × Fos-tTA/GFP mice, with an activity-dependent and Cre-dependent viral vector expressing an inhibitory DREADD, AAV_9.DIO.TRE.hM4Di.P2A. mCherry (ADCD).[25] In activated cholinergic neurons, tetracycline transactivator (tTA) will drive hM4Di and mCherry expression when mice are off doxycycline (DOX)-containing food. Injected mice were switched from a DOX-on to DOX-off diet, exposed to SAL, APP, or AV odor, then put back on DOX chow. Twenty-four hours later, mice were exposed to the same or a different odor and then processed for ChAT and GFP (to amplify the cFos-GFP signal) IHC (Figure 3A). This design enables VP cholinergic neurons activated on day 1 (i.e., test 1) to be $ChAT^+$ and $ADCD^+$, and neurons activated on day 2 (i.e., test 2) to be $ChAT^+$ and $cFos^+$.

Very few $ADCD^+$ or $cFos^+$ VP cholinergic neurons were detected in animals exposed and re-exposed to SAL (Figure 3B). Both the first exposure and the re-exposure to either the APP odor or the AV odor activated VP cholinergic neurons ($ChAT^+/ADCD^+$, $ChAT^+/cFos^+$; Figures 3C and 3D). Notably, in each case, virtually all of the $ADCD^+$ VP cholinergic neurons (activated during the first exposure) were also $cFos^+$ (reactivated during the second exposure).

In a distinct cohort of animals, we switched the second odor presented so that it was distinct from the first odor (i.e., from APP to AV or vice versa: Figure 4A). In these mice, we found that similar numbers of VP cholinergic neurons were activated during the first odor exposure ($ChAT^+/ADCD^+$, Figures 4B and 4C) and during the second odor exposure ($ChAT^+/cFos^+$, Figures 4B and 4C) as seen in the previous cohort (compare Figures 3C and 3D with Figures 4B and 4C). However, in these mice there were essentially no reactivated VP cholinergic neurons regardless of which odor was presented first (i.e., no $ADCD^+/cFos^+$ VP cholinergic neurons).

Importantly, the number of $ChAT^+$ neurons was not significantly different across experiments (Figure S5A), and both odors increased the number of $ADCD^+$ (Figure S5B) and $cFos^+$ (Figure S5C) neurons, regardless of which day the odor was presented. In sum, each odor significantly increased the number of activated VP cholinergic neurons compared to SAL (Figures S6A and S6B). However, the number of reactivated VP cholinergic neurons ($ChAT^+/ADCD^+/cFos^+$ neurons) was dependent on which odor was presented on day 2. If mice were exposed to the same odor on days 1 and 2, there was a significantly greater number of reactivated VP cholinergic neurons ($F(3, 17) = 68.8$, $p < 0.001$; Figure 4D, APP/APP and AV/AV compared to APP/AV and AV/APP), whereas if mice were exposed to a different odor on day 2, there was no overlap between $ChAT^+/ADCD^+$ and $ChAT^+/cFos^+$ VP cholinergic neurons. This indicates that VP cholinergic neurons that were activated in response to the first odor are not reactivated when mice are exposed to a distinct odor on day 2. We replicated these findings using the robust activity marking (RAM) system in C57 mice (Figures S7 and S8).

To further examine whether the activation of VP cholinergic neurons was odor specific or determined by valence, we repeated our ADCD/cFos labeling experiments using two distinct APP or AV odors (Figure S9). One cohort of mice was exposed to the APP odor (2-phenylethanol) on day 1 and exposed to another APP odor (peanut butter oil) 24-h later (day 2). In these mice, ~80% of VP cholinergic neurons activated on day 1 were reactivated on day 2 (Figures S9A and S9B). A second cohort of mice was exposed to the AV odor (mountain lion urine) on day 1 and exposed to a distinct AV odor (peppermint oil) on day 2. In these mice, ~70% of day-1-activated VP cholinergic neurons were reactivated (Figures S9C and S9D). These results indicate that the activation and reactivation of VP cholinergic neurons are valence specific and not due to the odors themselves.

Selective inhibition of VP cholinergic neurons previously activated by the APP odor abolishes and reverses approach behavior to the APP odor

To determine the participation of each specific subpopulation of VP cholinergic neurons in approach to the APP odor and/or avoidance of the AV odor, we used ADCD-hM4Di

to selectively silence VP cholinergic neurons that were previously activated by each odor (Figure 5A). As expected, in a preference test with the APP odor, mice in the sham group displayed the usual approach behavior to the APP odor (Figures 5B [left] and 5C). However, selective silencing of VP cholinergic neurons that were previously activated by exposure to the APP odor abolished this behavior ($t(11) = 2.72$, $p < 0.05$; Figures 5B [right] and 5C). Particularly striking was that inhibition of previously activated APP odor VP cholinergic neurons not only blocked approach behavior but in fact elicited active avoidance of the APP odor.

In a preference test with the AV odor, mice in the sham group displayed avoidance of the AV odor (Figures 5D [left] and 5E). In sharp contrast to the dramatic effects of silencing APP-odor-activated VP cholinergic neurons, mice with ADCD-hM4Di silencing of VP cholinergic neurons previously activated by exposure to the AV odor had no effect (Figures 5D [right] and 5E). These results underscore our findings using hM4Di for non-selective inhibition of VP cholinergic neurons (Figure 2) and were devoid of any changes in locomotor activity (Figure S10). Combined, our DREADD inhibition experiments show that inhibition of VP cholinergic neurons (either general silencing or selective inhibition of APP VP cholinergic neurons) reversed approach to the APP odor and led to active avoidance of the APP odor.

APP-vs. AV-odor-activated VP cholinergic neurons are intermingled but differ in certain electrophysiological properties, neuronal morphology, and projections to the BLA

We next examined features that might be shared and factors that might distinguish the two subpopulations of VP cholinergic neurons. First, for all mice assessed in Figures 3 and 4, we relocalized the site of ADCD injection and mapped APP- (Figure S11, blue circles) and AV-odor-responding (Figure S11, orange triangles) VP cholinergic neurons. Across the targeted regions (bregma +0.62 to +0.14), we found that these differentially activated subgroups of VP cholinergic neurons are spatially intermingled within the VP (Figure S11).

Next, to ask how the two subpopulations of VP cholinergic neurons might differ in electrophysiological properties from each other, we used a Cre-dependent activity marker (FLEX-RAM)[26] to label each population with ADCD as described above and then used patch-clamp recordings to quantify different aspects of the electrophysiological profile of each subpopulation (Figures 6A and 6B). Recordings were performed at least 3 days after odor exposure to avoid any transient changes in functional profile that might arise from acute neuronal activation. We compared the properties of APP- and AV-odor-activated VP cholinergic neurons to a pool of “non-activated” VP cholinergic neurons obtained from ChAT-tau-eGFP mice maintained in the home cage. Both APP and AV VP cholinergic neurons displayed a greater rate of maximum firing ($F(2, 38) = 10.71$, pairwise comparisons: ALL vs. APP $t(31) = 5.36$, $p < 0.01$; ALL vs. AV $t(27) = 2.80$, $p < 0.05$; Figure 6F) and sag potential (Figure S12A). Most other passive and active features were shared by control and odor-sensitive VP cholinergic neurons (Figure S12). However, there were important differences between APP- and AV-odor-activated VP cholinergic neurons that produced clear distinctions in their action potential profiles and their relative excitability (Figures 6C–6E). Specifically, AV-odor-activated VP cholinergic neurons were slightly more hyperpolarized

than APP-odor-activated VP cholinergic neurons ($F(2, 38) = 11.39$, $p < 0.001$; pairwise comparisons: APP vs. AV $t(18) = 2.72$, $p < 0.05$; Figures 6C and 6G). AV-odor-activated VP cholinergic neurons also had a smaller amplitude of the afterhyperpolarization potential ($F(2, 38) = 4.53$, $p < 0.05$; pairwise comparisons: APP vs. AV, $t = 2.74$, $p < 0.05$; Figures 6D and 6H). The net effect of the differences in these features underlies the phenotype that APP VP cholinergic neurons are less excitable than AV VP cholinergic neurons.

All cells examined by electrophysiological recordings were labeled with neurobiotin, relocalized and identified by post hoc ChAT IHC and by expression of FLEX-RAM. Relocalized neurons were reconstructed to assess the soma-proximal morphology of APP- and AV-odor-activated VP cholinergic neurons (Figure 6I). A convex hull analysis was conducted to assess the surface area and volume occupied by APP- vs. AV-odor-activated VP cholinergic neurons. The convex hull enveloping APP-odor-activated VP cholinergic neurons was smaller in surface area ($F(1, 10) = 12.22$, $p < 0.05$; Figure 6J) and volume (Figure S13C) compared to AV-odor-activated VP cholinergic neurons. APP-odor-activated VP cholinergic neurons also exhibited a significantly smaller dendrite area ($F(1, 10) = 26.77$, $p < 0.05$; Figure 6K) and dendrite volume ($F(1, 10) = 57.31$, $p < 0.05$; Figure 6L). In addition to these features, APP-odor-activated VP cholinergic neurons had a significantly greater number of intersecting points in a Sholl analysis at distances close to the soma (at 10 μm $F(1, 10) = -2.69$, $p < 0.05$; at 20 μm $F(1, 10) = -3.16$, $p < 0.05$; Figure 6M). Next, we assessed the percentage of reconstructed neurons whose dendrites reached a set distance from the soma in a Sholl analysis. The dendritic arbor of ~80% of AV-odor-activated VP cholinergic neurons extended at least 100 μm from the soma, whereas less than 20% of APP-odor-activated VP cholinergic neurons reached this distance (Figure 6N). Additional morphometric features that were not statistically different between APP- and AV-odor-activated VP cholinergic neurons are shown in Figure S13. Overall, these results consistently demonstrate APP-odor-activated VP cholinergic neurons are smaller and more complex in their proximal dendritic arbor than AV-odor-activated VP cholinergic neurons. These data, along with our slice electrophysiology profile of APP- and AV-odor-activated VP cholinergic neurons, are consistent with potential differences in circuit engagement.

The BLA is a major projection target of VP cholinergic neurons.[8,19] To begin to examine how these two distinct populations of VP cholinergic neurons might differ in their projections encoding valence, we examined the relative predominance (or lack thereof) of the APP vs. AV projections to the BLA (Figures 7A–7C and S14). Although we found an equal number of VP cholinergic neurons that were activated by the APP vs. AV odor (Figure 7D, left), the relative proportion of BLA-projecting APP vs. AV VP cholinergic neurons was not equivalent. The percentage of BLA-projecting VP cholinergic neurons that were activated by the AV odor was significantly greater than the number of BLA-projecting VP cholinergic neurons activated by the APP odor ($t(6) = -2.98$, $p < 0.05$; Figure 7D, right). This result underscores the predominance of AV encoding VP cholinergic projections to the BLA.

DISCUSSION

We identified two non-overlapping subpopulations of VP cholinergic neurons: one activated in response to APP odors and a second, distinct subpopulation activated in response to AV odors. We demonstrate that despite being activated in response to both odors, VP cholinergic neuron activity is absolutely required for approach behavior. These two subpopulations of VP cholinergic neurons also differ in passive and active electro-physiological properties, dendritic morphology, and projections to the BLA. These data are consistent with differential integration of each subpopulation into valence processing circuits.

VP cholinergic neurons are engaged in behavioral responses to both APP and AV odors

Few studies have examined how mice respond to innately pleasant stimuli. The APP odors used in the present study were 2-phenylethanol (the active component of rose oil)[27] and peanut butter oil. A previous experiment showed that although mice do not exhibit a preference for 2-phenylethanol, mice display anti-depressive-like behaviors.[27] We demonstrate here that mice display approach to the APP odor. One hypothesis for this difference is the arena in which the mice were tested. We used two arms of a Y-maze in which mice were given the ability to freely roam between two arms, likely leading to the exhibition of approach behavior. Although the VP has a well-established role in reward-related behaviors such as drug addiction,[11,28,29] the role of VP cholinergic neurons in reward behaviors is unclear. 192-IgG-saporin-induced lesions of cholinergic neurons in the nucleus accumbens (NAc) and VP reduced cocaine self-administration,[30] implicating VP cholinergic neurons in some aspect of reward-related behaviors. Our results show that VP cholinergic neurons are engaged following exposure to APP stimuli.

Mice reliably display innate avoidance behavior following predator odor exposure.[31–36] This behavior is consistent across multiple predator odors (fox urine, cat urine, mountain lion urine, 2,5-dihydro-2,4,5-trimethylthiazoline, or peppermint oil). Avoidance of predator odor is accompanied by numerous neurobiological changes. Among a wide array of effects, the most notable include cFos activation in brain regions related to stress,[37] the mPFC,[31] and the BLA.[38] The results from the current study add to these findings and, along with our previous work,[25] demonstrate that activation of VP cholinergic neurons is another reliable response following exposure to aversive odors.

VP cholinergic signaling is required for approach to the APP odor

Numerous studies have reported that approach behaviors are more readily manipulated than avoidance behaviors.[39–41] We show that general silencing of VP cholinergic neurons, as well as inhibiting APP-odor-activated VP cholinergic neurons, not only blocked approach behavior but led to avoidance of the APP odor. This suggests that avoidance may be the default behavior until mice encounter an APP stimulus that engages APP VP cholinergic neurons. Basal forebrain cholinergic neurons (BFCNs) outside of the VP have also been shown to play a role in behavioral responses to APP stimuli.[42–44] However, these previous studies focused on learned behaviors associated with rewarding stimuli as opposed to innate behaviors. We have previously found that distinct subsets of BFCNs govern learned vs. innate behavioral responses.[25] As such, VP cholinergic neurons may play a unique role

in innate behavioral responses to salient stimuli. While avoidance behaviors are governed by multiple circuits and are thus resistant to inhibition of a single component, approach behaviors are more susceptible to inhibition of VP cholinergic neurons.

Avoiding predators and noxious stimuli is crucial for survival. As such, the numerous brain regions and circuits known to be involved in avoidance of the predator odor[31–35,37,38,45] might provide redundancy and compensate for the inhibition of AV-odor-activated VP cholinergic neurons, thus preserving a behavior critical for survival. Cholinergic signaling from other BFCNs, as well as cholinergic signaling outside of the basal forebrain, also contributes to behavioral responses to AV stimuli.[25,46–53] These compensating brain regions and circuits (both cholinergic and non-cholinergic) may allow an animal to maintain continued avoidance of threatening stimuli despite the inhibition of VP cholinergic neurons.

Functional heterogeneity of VP cholinergic neurons

We identify two subpopulations of VP cholinergic neurons that are differentially activated by APP vs. AV odors. In addition to engagement in different behavioral responses, APP vs. AV VP cholinergic neurons exhibited differences in some electrophysi-ological features, morphology, and projections to the BLA. Changes in neuronal morphology and alterations in electrophysiological features are two common indicators of changes in the connectivity of neural circuits.[54–57] As the primary output of VP cholinergic neurons targets the BLA,[8,19] we chose to examine the proportion of BLA-projecting VP cholinergic neurons activated by each odor. Our retrograde mapping experiment revealed that a greater percentage of BLA-projecting VP cholinergic neurons were activated by AV odors. Collectively, these results illustrate the presence of two distinct non-overlapping subpopulations of cholinergic neurons in the VP, demonstrating functional heterogeneity of VP cholinergic neurons.

The two subpopulations of VP cholinergic neurons identified in the present study resemble VP GABA (increased firing in response to a positive valence stimulus) and VP glutamate neurons (increased firing in response to a negative valence stimulus).[9] GABA neurons are the primary cell type within the VP, accounting for ~75% of all VP neurons.[17] VP GABA neurons have reciprocal connections with the NAc and project to the lateral hypothalamus, thalamus, and ventral tegmental area (VTA).[8,58,59] Importantly, VP GABA neurons have a crucial role in reward processing. Activating VP GABA neurons is reinforcing,[9,17,60] and VP GABA neurons demonstrate increased calcium activity in response to reward-predictive cues.[59] Furthermore, inhibiting VP GABA neurons decreases reward seeking.[9,59] The behavioral effects of inhibiting VP cholinergic neurons and loss of approach to APP odors resembled the reported effect of inhibiting VP GABA neurons. This raises the possibility that VP cholinergic neurons co-release GABA, a feature of other BFCNs that corelease GABA and acetylcholine in the cortex.[61] It remains to be seen whether the same is true for VP cholinergic neurons.

Glutamatergic neurons represent ~15% of all cells within the VP.[17] VP glutamatergic neurons have reciprocal connections with the BLA, receive input from the NAc and cortex, and send projections to the VTA.[8,62] In contrast to VP GABA neurons, VP glutamatergic neurons play a prominent role in aversive behaviors.[9,17,60,62] VP glutamatergic neurons were previously found to lack markers of cholinergic neurons.[62] However, another study

demonstrated co-expression of vGLUT3 mRNA in BFCNs that project to the BLA,[63] and a recent study has shown expression of vGLUT3 in VP/substantia innominata (SI) cholinergic neurons that project to the BLA.[64] Our results show that a significantly greater percentage of BLA-projecting VP cholinergic neurons are activated by the AV odor. It is possible that these VP cholinergic neurons co-express glutamatergic markers. Co-expression of VP cholinergic neurons with GABA or glutamate (and, potentially, other markers) remains an intriguing area for future research.

Numerous studies have reported the activation of BFCNs following exposure to both rewarding and aversive stimuli.[9,20,53] Although VP cholinergic neurons were hypothesized to resemble other BFCNs and encode salience, we show that cholinergic projection neurons of the VP are functionally complex and can encode valence of olfactory stimuli. An important difference between our study and previous ones is the stimuli presented. While other studies have used APP and AV stimuli of distinct sensory modalities, we chose to specifically utilize APP and AV stimuli of the same sensory modality. In contrast to previous studies,[9,20] we did not assess how VP cholinergic neurons respond to cues predicting odor delivery. Future studies are needed to examine how VP cholinergic neurons respond to stimuli of distinct sensory modalities and how they respond to cues predicting APP and AV odors.

Functional diversity of BFCNs

Cholinergic neurons in the VP as well as in the nucleus basalis of Meynert (nBM), medial septum/vertical limb of the diagonal band (MS/vDB), horizontal limb of the diagonal band (hDB), and SI comprise BFCNs.[53] BFCNs originate from various neurogenic zones and at different times in the embryonic brain.[53,65] Although in general birth date and location correlate with the final projection targets in the adult brain, our understanding of the functional differences between these populations is just beginning to emerge. For example, cholinergic projections from the nBM to the BLA play a role in both cue-associated fear learning[25,46–48,66] and reward learning.[42,52] Cholinergic projections from the MS/vDB to the hippocampus have been heavily implicated in behavioral responses to stress and anxiety[49,67–69] and reward learning.[43,44] Our findings add to this growing understanding by demonstrating that there are distinct subpopulations of VP cholinergic neurons that can mediate behavioral responses to either innately positive or negative valence stimuli.

Conclusions and future directions

Despite the well-established role of the VP in valence processing, prior studies have not tested the participation of VP cholinergic neurons in valence encoding. Our results demonstrate that VP cholinergic neurons are activated in response to either APP or AV odors. This present study focused specifically on the functional heterogeneity of VP cholinergic neurons. Future research can determine whether these results extend to valence of other sensory stimuli (i.e., taste and touch) and to learned (i.e., conditioned) responses. Future studies can examine potential differences in other brain regions that receive cholinergic input from the VP (mPFC and medial dorsal thalamus). Another area for future research is to determine how valence-encoding VP cholinergic neurons interact with valence-encoding neurons of the BLA and/or other regions to promote approach

vs. avoidance behaviors. Targeting positive vs. negative valence-encoding microcircuits may lead to the development of more efficacious pharmacotherapeutic treatments for neuropsychiatric disorders characterized by misattributions of valence and/or motivational imbalance.

Limitations of the study

Previous studies examining the role of VP GABAergic and glutamatergic neurons in approach and avoidance behaviors used *in vivo* electrophysiology recordings[9,62] or *in vivo* calcium imaging.[18,59] These imaging modalities track the activity of VP neurons with greater temporal resolution than the activity-dependent fluorescent reporters used here. As such, we cannot distinguish whether VP cholinergic neurons have a more nuanced role in approach or avoidance behaviors. Moreover, our method is reliant on, and limited by, the accuracy of virus injection and spread of the virus, likely under-representing the involvement of VP cholinergic neurons in approach and avoidance behaviors. Another limitation in our approach was that we did not account for potential differences in olfactory processing of APP and AV odors. Odors are sensed by sensory neurons in the vomeronasal system, which project to the olfactory bulb. Connections between the olfactory bulb and other parts of the brain determine the valence of odors.[70,71] Behavioral responses to odors also depend on spontaneous and experience-dependent activity of olfactory sensory neurons.[70] Differences in olfactory processing of the APP or AV odor may influence behavioral responses to odor exposure.

STAR★METHODS

RESOURCE AVAILABILITY

Lead contact—Further information and requests for resources and reagents should be directed to and will be fulfilled by the Lead Contact, David Talmage (David.Talmage@NIH.gov).

Materials availability—This study did not generate new unique reagents.

Data and code availability

- All data reported in this paper will be shared by the lead contact upon request.
- Original code used for analysis is freely available:

Fiber photometry:

https://github.com/rokim01/Fiber-Photometry-analysis

https://zenodo.org/records/10723901

Electrophysiology:

https://github.com/nsdesai/patch_clamp_analysis

https://zenodo.org/records/10723870

- Any additional information required to reanalyze the data reported in this paper is available from the lead contact upon request.

EXPERIMENTAL MODEL AND STUDY PARTICIPANT DETAILS

8–12 week-old male and female mice were randomly assigned to groups at the start of all experimental procedures. The strains of mice used were: C57BL/6J (Jax #000664), Chat-IRES-Cre:Δneo (B6; 129S6-Chattm2(cre)Lowl/J; Jax # 006410, abbreviated Chat-Cre), and the offspring of Chat-Cre mice crossed to Fos-tTA/Fos-shEGFP mice, (B6. Cg-Tg(Fos-tTA, Fos-EGFP*)1Mmay/J; Jax # 018306, abbreviated Chat-Cre x Fos-tTA/GFP). Chat-tau-eGFP mice (a gift from S.Vijayaraghavan, University of Colorado),[74] which express GFP in all cholinergic neurons and processes, were used as naive home-cage controls in electrophysiology experiments. Previous studies indicate the electrophysiological profile of neither Chat-tau-eGFP or Chat-Cre mice differ from non-genetically tagged cholinergic neurons.[75] All mice were housed in a 12-h light/dark cycle with temperature and humidity control. Food and water were available *ad-libitum*. All procedures were approved by the NINDS Animal Care and Use Committee (ASP # 1531). For all experiments, the APP odor used was 2-phenylethanol (Sigma # 77861), and the AV odor used was mountain lion urine (Predator Pee # 92016). Commercially available peanut-butter oil was used as a distinct APP odor, and peppermint oil (Sigma # 77411) was used as a distinct AV odor.

METHODS DETAILS

Surgery—Mice were anesthetized using isoflurane (3–5% induction, 1.5% maintenance) and placed in a stereotax. Bilateral injections targeted the VP using coordinates from the Paxinos Mouse Brain Atlas (AP +0.38, ML +/− 1.45, DV5.0). A Hamilton syringe was slowly lowered to the VP and mice were injected with ~0.3 μL of the following viral vectors dependent on experiment: AAV_9.DIO.TRE.hM4Di.P2A.m.Cherry (ADCD; packaged at UNC viral vector core),[25] AAV_9.RAM.d2tTA.TRE.mCherry.NLS-FLAG (RAM; Addgene # 63931, packaged at UNC viral vector core),[26] AAV_9.Syn.Flex-GCaMP6f.WPRE.SV40 (GCaMP6f; Addgene # 100837), AAV_8.hSyn.DIO.hM4Di (Gi).mCherry (hM4Di; Addgene # 44362), AAV_9.eSyn.eGFP (Vector Biolabs # VB4870), AAV_9.RAM.d2tTA.TRE.Flex.tdTomato (FLEX-RAM; Addgene # 84468, packaged at NINDS Viral Vector Core). For retrograde tracing experiments, 0.15 μL Fast Blue (Polysciences # 17740-1) was injected bilaterally in the BLA (AP −1.35, ML +/− 3.2, DV 4.7). For optical recording of calcium signaling, *in vivo* fiber photometry was used. A fiber optic cannula (Neurophotometrics, ferrule diameter 1.25 mm, core diameter 400 μm) was implanted ~100 μm above the VP virus injection site and secured using dental cement.

Odor preference behavior tests—All experiments assessing the behavioral responses to odors were conducted using a near-infrared (NIR) modular Y-Maze with a NIR camera (Med Associates). Initial odor preference was assessed in a single 10-min session. One arm of the Y-Maze contained an odor (either APP or AV) on a gauze pad and one arm contained SAL. Mice began the session in the third vacant arm. After initial entry into either the odor-containing or SAL-containing arm, re-entry into the starting arm was blocked, forcing mice to choose between the odor vs. SAL arm. Time spent in each arm (odor vs. SAL) was analyzed using EthoVision XT (v 15) software.

ADCD/RAM labeling of activated VP cholinergic neurons—For ADCD and RAM labeling experiments, Chat-Cre x Fos-tTA/GFP mice were given approximately 3–4 weeks to recover from surgery post viral injection. Following recovery, behavior sessions occurred over three consecutive days. On the first day (Day 0), mice were habituated twice to the Y-Maze. During each habituation session, mice were allowed to explore only one arm of the Y-Maze for 10 min, counter-balanced for each arm of the Y-Maze. Following the second habituation session, mice were transferred to a clean cage and removed from a DOX diet, thus allowing for ADCD or RAM expression. On Day 1, approximately 24-h later, mice were exposed to either an odor or SAL in one arm of the Y-maze (labeling activated VP cholinergic neurons). Following ADCD or RAM labeling of activated VP neurons, mice were returned to a DOX diet. On Day 2, approximately 24-h later, mice were then exposed to either SAL or an odor in a different arm of the Y-Maze. Mice were returned to the home cage until tissue was collected for additional processing. We have previously shown that ADCD expression is observed 72-h post-stimulus presentation.[25] A previous experiment demonstrated RAM expression does not decay for at least 2 weeks.[26] Therefore, at the timepoint in our experiments when mice are collected for tissue processing, (on Day 2, 24-h after ADCD or RAM labeling of activated VP neurons), we expect ADCD and RAM expression to be observed 24-h following odor presentation, and potential decay in fluorescence not a confounding factor in our results.

DREADD inhibition experiments—Odor preference was assessed following general inhibition of VP cholinergic neurons using a floxed inhibitory DREADD in Chat-Cre mice (hM4Di), or inhibition of previously activated VP cholinergic neurons (ADCD-hM4Di) in Chat-Cre x Fos-tTA/GFP mice. For hM4Di odor preference tests, mice were allowed to recover from surgery for 3–4 weeks and then injected IP with 0.1 mg/kg clozapine. Approximately 15-min later, odor preference was assessed in the Y-Maze, identical to the odor preference test described above. For ADCD labeling in odor preference tests, mice were allowed to habituate to the Y-Maze on Day 0 and activated VP cholinergic neurons were labeled with ADCD on Day 1. For selective inhibition of previously activated VP cholinergic neurons on Day 2, mice were injected with 0.1 mg/kg clozapine and allowed to explore two arms of the Y-Maze (previously exposed odor vs. SAL). Time spent in each arm (odor vs. SAL) was analyzed using Ethovision software.

In-vivo calcium signaling assays using fiber photometry—Chat-Cre mice were injected with a Cre-dependent GCaMP6f in the VP and a fiber optic cannula was implanted above the viral injection site. Fiber photometry recordings were made using the Neurophotometrics FP3002 system. Acquisition parameters were: 415 (for isobestic channel recordings) and 470 (GCaMP channel recordings) nm channels, 20 frames/sec, power ~100 μw. All fiber photometry recordings were conducted in behavior chambers equipped with an odor delivery system (Med Associates). Mice were given two days to habituate to the behavior chamber and patch cords. Mice were then exposed to timed delivery of either odor (APP or AV). Timed odor delivery took place in a 10-min session, where odor was delivered (3 × 10 s) every 3 min. Approximately 24-h following the first odor exposure session, mice were exposed to the opposite odor.

Processing of all fiber photometry data was performed using a custom MATLAB script. Initialization frames (×5 s at the start of recordings) were removed from the raw data and raw fluorescence values were binned at 5 Hz intervals. The GCaMP signal was then normalized to the isobestic signal and fluorescence measures were obtained. The change in fluorescence (ΔF/F) was calculated and converted to Z-scores. The integrated Z score vs. time was estimated by the area under the curve (AUC), calculated using GraphPad Prism representing a single value combining fluorescence intensity and time. The max Z score ΔF/F was defined as the highest Z score ΔF/F during the 10 s odor delivery period.

Immunohistochemistry (IHC)—Following behavior testing or odor exposure (~45 min for C57/BL6J and Chat-Cre mice; ~2.5 h for Chat-Cre x Fos tTA/GFP mice), mice were perfused with phosphate buffered saline (PBS) and 4% paraformaldehyde (PFA). 30–60 min post-stimulus presentation is a standard protocol for assessing cFos using immunohistochemistry.[76] In Fos tTA/GFP mice, although the induction of endogenous Fos protein is ~45 min, we perfused these mice at ~2.5 h to account for the maturation of GFP protein. Previous studies have demonstrated the number of activated cells identified by Fos-GFP fluorescence is maximal at 2–3 h post-stimulation.[77,78] Brains were post-fixed in 4% PFA overnight before being cryoprotected in 30% sucrose. 50 μm slices were cut on a cryostat and stored in 50% PBS/glycerol at −20°C until immunostaining.

For all experiments, free floating slices were first washed (3 × 10 min) in PBS +2% Triton X-100 (PBST). Slices were then transferred to a blocking solution containing PBST and 10% normal donkey serum (NDS) and incubated on a shaker for 2-h at room temperature. Following blocking, slices were incubated overnight at 4°C in blocking solution with the addition of the following antibodies (dependent on experiment): goat anti-ChAT (Millipore Sigma AB144P), rabbit anti-cFos (Synaptic System 226 008), chicken anti-GFP (Abcam ab13970), mouse anti-mCherry (Living Colors 632543), or rat anti-Substance P (Millipore Sigma MAB356). All primary antibodies were used at 1:500. Following incubation with primary antibodies, slices were washed (3 × 10 min) in PBST and then incubated (2-h at room temperature) in blocking solution with the addition of the following secondary antibodies (dependent on primary antibody used, all secondary antibodies were used at 1:1000): donkey anti-goat A647 (Thermo Fisher A-21447), donkey anti-rabbit A488 (Thermo Fisher A-21206), donkey anti-chicken A488 (Jackson Immuno 703-545-155), donkey anti-mouse A594 (Thermo Fisher A-21203) or donkey anti-rat A594 Thermo Fisher A-21209). Following incubation with secondary antibodies, slices were first washed in PBST (3 × 10 min) and then washed in PBS (1 × 10 min). Slices were mounted onto slides using Fluoromount-G with DAPI (Southern BioTech 0100-01).

All images were acquired on an Olympus VS200 slide scanner with a Hamamatsu Orca-Fusion camera. Whole slice images were obtained using the 415, 470, 594 and 647 nm channels. Each image was acquired using 5 μm z-steps and identical exposure times for each channel. Images were saved as.vsi files before being converted to Imaris files for analysis.

Electrophysiology—To assess passive and active electrophysiological properties of VP cholinergic neurons previously been activated in response to the APP or AV odor, we first labeled odor responsive neurons *in vivo* with the permanent activity marker FLEX-RAM

(Addgene # 84468).[26] FLEX-RAM is identical to RAM (i.e., activity dependent expression only went off a DOX diet) but is only expressed neurons that contain Cre-recombinase. Therefore, Chat-Cre mice were injected with FLEX-RAM in the VP and exposed to either the APP or AV odor 3–4 weeks later (identical to the ADCD and RAM labeling experiments described above). Following odor exposure, mice were returned to a DOX diet and stayed in the home cage until electrophysiology recordings were conducted (a minimum of 3 days, maximum of 21 days). Odor naive mice of Chat-tau-eGFP genetic background were used as non-odor exposed controls. Following a minimum of 72 h, mice were euthanized, the brain was removed, and 300 mm slices containing the VP were taken on a Leica VT1200 vibratome (details discussed below). A previous experiment validating the RAM construct showed peak RAM expression lasts 1-week post-stimulation, begins to decay at 2 weeks and is no longer observed 4 weeks post-stimulation.[26] It is possible that RAM expression is declined in slices that were recorded at later timepoints in our study (2–3 weeks). However, since we are only assessing long-lasting changes in electrophysiological properties recorded from cells with visible RAM expression, we do not expect this potential decay in RAM expression to affect our electrophysiology results.

Brain slices containing the VP were prepared using standard procedures.[75,79] Shortly after receiving a lethal dose of ketamine/ xylazine, mice were perfused transcardially with an ice-cold cutting solution containing (in mM): 92 N-methyl-D-glucamine, 2.5 KCl, 1.25 NaH_2PO_4, 30 $NaHCO_3$, 20 HEPES, 25 D-glucose, 2 thiourea, 5 ascorbate, 3 pyruvate, 0.5 $CaCl_2$, and 10 $MgSO_4$. Brains were removed as rapidly as possible, and a Leica VT1200 vibratome was used to make 300-μm-thick coronal sections. Slices were cut in the same ice-cold saline used for perfusion and were then transferred to a covered chamber filled with a holding solution containing (in mM): 92 NaCl, 2.5 KCl, 1.25 NaH_2PO_4, 30 HEPES, 25 D-glucose, 2 thiourea, 5 ascorbate, 3 pyruvate, 2 $CaCl_2$, and 2 $MgSO_4$. Slices were kept in this solution at room temperature for 1–2 h before being transferred to the stage of an upright microscope for patch clamp recording. Slices were then continually perfused with an artificial CSF kept at 31°C and containing (in mM): 125 NaCl, 2.5 KCl, 1.25 NaH_2PO_4, 25 $NaHCO_3$, 10 D-glucose, 2 $CaCl_2$, and 1 $MgCl_2$. All three solutions (cutting, holding, recording) were bubbled with 95% O_2/5% CO_2 to maintain pH at ~7.4; all had osmolarities of 305–315 mOsm.

Patch clamp recordings were obtained at physiologic temperature (~31°C) under visual guidance using patch electrodes (3–7 MΩ) filled with an internal solution containing (in mM): 125 K-gluconate, 10 KCl, 4 NaCl, 10 HEPES, 4 Mg-ATP, 0.3 Tris-GTP, 7 phosphocreatine (pH 7.4, osmolarity 290 mOsm), and 0.2% neurobiotin. Before patching, fluorescence images (GFP or tdTomato) were taken with a high-resolution CCD camera to establish neuronal identity. Recordings were made in current clamp mode with bridge balance and pipette capacitance neutralization parameters set appropriately. Membrane potentials were not corrected for junction potential, which was approximately 10 mV given these solutions. Recordings with series resistances >25 MΩ, input resistances <50 MΩ, and resting potentials >−50 mV were discarded, as were recordings where any of these parameters changed by more than 20%.

To assess intrinsic excitability, neurons were held at a baseline potential of −65 mV by a DC injection, and a family of current steps (500 ms duration, −60 to 200 pA amplitude) were injected. Steps were separated by 10 s. To assess subthreshold resonance, swept-sine currents ("chirp") between 0.5 and 12 Hz were injected (using MATLAB function *chirp*), averaged, and used to extract impedance.

Neuronal morphology—VP slices that contained neurobiotin filled cells were stored in 4% PFA overnight following electrophysiology recordings. Slices were then kept in PBS until immunostaining. The immunostaining protocol was identical to the immunostaining procedures described above. The primary antibody used was goat anti-ChAT (1:500, Millipore Sigma AB144P). The secondary antibodies used were donkey anti-goat A488 (Invitrogen A-11055) and streptavidin conjugated to Alexa Fluor 594 (Thermo Fisher S32356) to visualize neurobiotin. All images were acquired on a Nikon spinning disk confocal microscope using the following parameters: 405/488/594/647 lasers, minimal laser power (>10%), identical exposure times for each channel, 4x averaging and 0.5 μm z-steps. All images were converted to Imaris files and the filaments tab within Imaris was used for automated neuronal tracing and analysis, including convex hull measurements and sholl analysis.

QUANTIFICATION AND STATISTICAL ANALYSIS

All odor preference behavior videos were first converted to.mP4 files and uploaded to Ethovision (v.15 from Noldus). The Y-Maze dimensions were used to delineate the arena borders and each arm containing an odor or SAL gauze pad was outlined as a zone. Automated rodent tracking was used for each video and the time (in seconds) the mouse spent in each zone was obtained. We did not note any sex differences in approach or avoidance behaviors in response to odor exposure.

A pipeline for image analysis and quantification using Imaris is depicted in Figure S2. To assist in defining VP boundaries, immunostaining for Substance P, which demarcates VP borders[8,17] was conducted in brain slices from a Chat-tau-eGFP mouse (Figure S2). These boundaries were then used in later slices to delineate the VP. The whole VP was selected as the ROI for analysis. Whole slice images were first cropped and borders delineating the VP were created to mask any signal outside of the VP. Representative, nonbinary fluorescent images containing the VP is shown in Figure S4. The VP was identified as the brain region containing a sparse cluster of cholinergic neurons ventral to the anterior commissure and striatum, and dorsal to the densely packed cluster of cholinergic neurons in the hDB. Within Imaris, the spots and surfaces function were used to create size and/or intensity-based thresholds for each channel. The colocalization tab was used to create a new channel with the colocalized signal between two defined channels. All data containing the total number of spots or surfaces was then exported. For each mouse, the total number of spots, surfaces and the colocalization of spots and surfaces, were obtained from 4 - 6 slices containing the VP (ranging from bregma +0.62 to +0.14). A mean cell count within the VP for each mouse was obtained by averaging the total number of cell counts across these slices.

For electrophysiology data, eighteen features were extracted from each cell recorded before and in the response to currents steps. (1) Membrane potential (mV), measured in the absence of a current injection. (2) Sag potential (mV), measured in response to a −60 pA step, equal to the difference between the steady-state potential and minimum potential. (3) Input resistance (MΩ), measured by the response to a −20 pA step. (4) Membrane time constant Tau (τ in ms), measured by the relaxation to a −20 pA step. (5) Rheobase (pA), the minimum current step of 500 ms duration needed to elicit an action potential. (6) Spike threshold (mV), measured from the first action potential of the rheobase current step ("first action potential"), and defined as the potential at which dV/dt crosses 20 mV/ms (7) Spike amplitude (mV), measured from the first action potential, and defined as the difference between spike threshold and the peak of the action potential. (8) Spike width (ms), measured from the first action potential at rheobase and defined as the width at half maximum (halfway between threshold and peak). (9) Spike latency (ms), measured at rheobase current, and defined as the time difference between the start of the step and the threshold crossing of the first step. (10) Upstroke (mV/ms), the maximum value of dV/dt on the upstroke of the first action potential at rheobase (11) Downstroke (mV/ms), the minimum value of dV/dt on the downstroke of the first action potential at rheobase. (12) AHP amplitude (mV), measured following the first action potential at rheobase, defined as the difference between threshold and the minimum potential 100 ms later. (13) AHP latency (ms), the time after spike threshold is crossed by the first action potential and the AHP minimum at rheobase. (14) AHP width (ms), the time difference at half maximum of the first AHP. (15) f-I slope (Hz/pA), the slope of the initial linear section of the f-I curve. (16) Max firing rate (Hz), the maximum firing rate produced by a current step between 0 and 200 pA, across the entire 500 ms duration. (17) Adaptation index (dimensionless), for the maximal current step, the number of spikes elicited in the second half of the 500 ms step divided by the number elicited in the first 250 ms. (18) Coefficient of variation (CV) of interspike intervals, measured from the maximal current step.

All statistical tests were conducted using GraphPad Prism (v. 9) or SigmaPlot (v. 14). When comparing two groups a two-tailed t-test was used and when comparing three groups a one-way ANOVA was used. For electrophysiology and neuronal morphology data, a nested ANOVA was run to account for replicate values obtained from the same mouse. Shapiro-Wilk and Smirnov-Kolmogorov tests were used to assess normality of the data. Non-parametric tests were conducted if the data failed these tests. For all statistical analysis, α was set at 0.05 and power was >0.8.

Supplementary Material

Refer to Web version on PubMed Central for supplementary material.

ACKNOWLEDGMENTS

This work was supported by funds from the National Institute of Neurological Disorders and Stroke Intramural Research Program (1ZIANS009424 to D.A.T., 1ZIANS009416 and 1ZIANS009422 to L.W.R.). We thank Taylor Muir for breeding and colony management of animals used in the study, and Dr. Prithiviraj Rajebhosale for insightful discussions. We also thank Dr. Ron Yu for technical assistance with odor delivery experiments. Biorender was used to prepare the graphical abstract.

REFERENCES

1. Tye KM (2018). Neural Circuit Motifs in Valence Processing. Neuron 100, 436–452. 10.1016/j.neuron.2018.10.001. [PubMed: 30359607]
2. Smith DM, and Torregrossa MM (2021). Valence encoding in the amygdala influences motivated behavior. Behav. Brain Res 411, 113370. 10.1016/j.bbr.2021.113370. [PubMed: 34051230]
3. Warlow SM, and Berridge KC (2021). Incentive motivation: 'wanting' roles of central amygdala circuitry. Behav. Brain Res 411, 113376. 10.1016/j.bbr.2021.113376. [PubMed: 34023307]
4. Kalivas PW, and Volkow ND (2005). The neural basis of addiction: a pathology of motivation and choice. Am. J. Psychiatry 162, 1403–1413. 10.1176/appi.ajp.162.8.1403. [PubMed: 16055761]
5. Fox ME, and Lobo MK (2019). The molecular and cellular mechanisms of depression: a focus on reward circuitry. Mol. Psychiatry 24, 1798–1815. 10.1038/s41380-019-0415-3. [PubMed: 30967681]
6. Farrell MR, Esteban JSD, Faget L, Floresco SB, Hnasko TS, and Mahler SV (2021). Ventral Pallidum GABA Neurons Mediate Motivation Underlying Risky Choice. J. Neurosci 41, 4500–4513. 10.1523/jneurosci.2039-20.2021. [PubMed: 33837052]
7. Lederman J, Lardeux S, and Nicola SM (2021). Vigor Encoding in the Ventral Pallidum. eNeuro 8, ENEURO.0064-21.2021. 10.1523/eneuro.0064-21.2021.
8. Root DH, Melendez RI, Zaborszky L, and Napier TC (2015). The ventral pallidum: Subregion-specific functional anatomy and roles in motivated behaviors. Prog. Neurobiol 130, 29–70. 10.1016/j.pneurobio.2015.03.005. [PubMed: 25857550]
9. Stephenson-Jones M, Bravo-Rivera C, Ahrens S, Furlan A, Xiao X, Fernandes-Henriques C, and Li B (2020). Opposing Contributions of GABAergic and Glutamatergic Ventral Pallidal Neurons to Motivational Behaviors. Neuron 105, 921–933.e5. 10.1016/j.neuron.2019.12.006. [PubMed: 31948733]
10. Castro DC, Cole SL, and Berridge KC (2015). Lateral hypothalamus, nucleus accumbens, and ventral pallidum roles in eating and hunger: interactions between homeostatic and reward circuitry. Front. Syst. Neurosci 9, 90. 10.3389/fnsys.2015.00090. [PubMed: 26124708]
11. Smith KS, Tindell AJ, Aldridge JW, and Berridge KC (2009). Ventral pallidum roles in reward and motivation. Behav. Brain Res 196, 155–167. 10.1016/j.bbr.2008.09.038. [PubMed: 18955088]
12. Gardner EL (2011). Addiction and brain reward and antireward pathways. Adv. Psychosom. Med 30, 22–60. 10.1159/000324065. [PubMed: 21508625]
13. McGovern DJ, and Root DH (2019). Ventral pallidum: a promising target for addiction intervention. Neuropsychopharmacology 44, 2151–2152. 10.1038/s41386-019-0528-z. [PubMed: 31558771]
14. Knowland D, Lilascharoen V, Pacia CP, Shin S, Wang EHJ, and Lim BK (2017). Distinct Ventral Pallidal Neural Populations Mediate Separate Symptoms of Depression. Cell 170, 284–297.e18. 10.1016/j.cell.2017.06.015. [PubMed: 28689640]
15. Liu B, Cao Y, Wang J, and Dong J (2020). Excitatory transmission from ventral pallidum to lateral habenula mediates depression. World J. Biol. Psychiatry 21, 627–633. 10.1080/15622975.2020.1725117. [PubMed: 32009492]
16. Ji Y-W, Shen Z-L, Zhang X, Zhang K, Jia T,Xu X, Geng H, Han Y, Yin C, Yang J-J, et al. (2023). Plasticity in ventral pallidal cholinergic neuron-derived circuits contributes to comorbid chronic pain-like and depression-like behaviour in male mice. Nat. Commun 14, 2182. 10.1038/s41467-023-37968-x. [PubMed: 37069246]
17. Faget L, Zell V, Souter E, McPherson A, Ressler R, Gutierrez-Reed N, Yoo JH, Dulcis D, and Hnasko TS (2018). Opponent control of behavioral reinforcement by inhibitory and excitatory projections from the ventral pallidum. Nat. Commun 9, 849. 10.1038/s41467-018-03125-y. [PubMed: 29487284]
18. Heinsbroek JA, Bobadilla AC, Dereschewitz E, Assali A, Chalhoub RM, Cowan CW, and Kalivas PW (2020). Opposing Regulation of Cocaine Seeking by Glutamate and GABA Neurons in the Ventral Pallidum. Cell Rep. 30, 2018–2027.e3. 10.1016/j.celrep.2020.01.023. [PubMed: 32049028]

19. Záborszky L, Gombkoto P, Varsanyi P, Gielow MR, Poe G, Role LW, Ananth M, Rajebhosale P, Talmage DA, Hasselmo ME, et al. (2018). Specific Basal Forebrain-Cortical Cholinergic Circuits Coordinate Cognitive Operations. J. Neurosci 38, 9446–9458. 10.1523/jneurosci.1676-18.2018. [PubMed: 30381436]
20. Hangya B, Ranade SP, Lorenc M, and Kepecs A (2015). Central Cholinergic Neurons Are Rapidly Recruited by Reinforcement Feedback. Cell 162, 1155–1168. 10.1016/j.cell.2015.07.057. [PubMed: 26317475]
21. Kucinski A, Avila C, and Sarter M (2022). Basal Forebrain Chemogenetic Inhibition Converts the Attentional Control Mode of Goal-Trackers to That of Sign-Trackers. eNeuro 9, ENEURO.0418-22.2022. 10.1523/eneuro.0418-22.2022.
22. Jin J, Cheng J, Lee KW, Amreen B, McCabe KA, Pitcher C, Liebmann T, Greengard P, and Flajolet M (2019). Cholinergic Neurons of the Medial Septum Are Crucial for Sensorimotor Gating. J. Neurosci 39, 5234–5242. 10.1523/jneurosci.0950-18.2019. [PubMed: 31028115]
23. Jiang YY, Zhang Y, Cui S, Liu FY, Yi M, and Wan Y (2018). Cholinergic neurons in medial septum maintain anxiety-like behaviors induced by chronic inflammatory pain. Neurosci. Lett 671, 7–12. 10.1016/j.neulet.2018.01.041. [PubMed: 29410218]
24. Chen L, Yin D, Wang TX, Guo W, Dong H, Xu Q, Luo YJ, Cherasse Y, Lazarus M, Qiu ZL, et al. (2016). Basal Forebrain Cholinergic Neurons Primarily Contribute to Inhibition of Electroencephalogram Delta Activity, Rather Than Inducing Behavioral Wakefulness in Mice. Neuropsychopharmacology 41, 2133–2146. 10.1038/npp.2016.13. [PubMed: 26797244]
25. Rajebhosale P, Ananth MR, Kim R, Crouse R, Jiang L, López-Hernńndez G, Zhong C, Arty C, Wang S, Jone A, et al. (2024). Functionally refined encoding of threat memory by distinct populations of basal forebrain cholinergic projection neurons. Elife 13, e86581. 10.7554/eLife.86581. [PubMed: 38363713]
26. Sørensen AT, Cooper YA, Baratta MV, Weng FJ, Zhang Y, Ramamoorthi K, Fropf R, LaVerriere E, Xue J, Young A, et al. (2016). A robust activity marking system for exploring active neuronal ensembles. Elife 5, e13918. 10.7554/eLife.13918. [PubMed: 27661450]
27. Ueno H, Shimada A, Suemitsu S, Murakami S, Kitamura N, Wani K, Matsumoto Y, Okamoto M, and Ishihara T (2019). Anti-depressive-like effect of 2-phenylethanol inhalation in mice. Biomed. Pharmacother 111, 1499–1506. 10.1016/j.biopha.2018.10.073. [PubMed: 30415864]
28. Ottenheimer DJ, Bari BA, Sutlief E, Fraser KM, Kim TH, Richard JM, Cohen JY, and Janak PH (2020).A quantitative reward prediction error signal in the ventral pallidum. Nat. Neurosci 23, 1267–1276. 10.1038/s41593-020-0688-5. [PubMed: 32778791]
29. Morales I, and Berridge KC (2020). Liking' and 'wanting' in eating and food reward: Brain mechanisms and clinical implications. Physiol. Behav 227, 113152. 10.1016/j.physbeh.2020.113152. [PubMed: 32846152]
30. Smith JE, Co C, Yin X, Sizemore GM, Liguori A, Johnson WE 3rd, and Martin TJ (2004). Involvement of cholinergic neuronal systems in intravenous cocaine self-administration. Neurosci. Biobehav. Rev 27, 841–850. 10.1016/j.neubiorev.2003.11.002. [PubMed: 15019433]
31. Hwa LS, Neira S, Pina MM, Pati D, Calloway R, and Kash TL (2019). Predator odor increases avoidance and glutamatergic synaptic transmission in the prelimbic cortex via corticotropin-releasing factor receptor 1 signaling. Neuropsychopharmacology 44, 766–775. 10.1038/s41386-018-0279-2. [PubMed: 30470839]
32. Pérez-Gómez A, Bleymehl K, Stein B, Pyrski M, Birnbaumer L, Munger SD, Leinders-Zufall T, Zufall F, and Chamero P (2015). Innate Predator Odor Aversion Driven by Parallel Olfactory Subsystems that Converge in the Ventromedial Hypothalamus. Curr. Biol 25, 1340–1346. 10.1016/j.cub.2015.03.026. [PubMed: 25936549]
33. Wu YP, Gao HY, Ouyang SH, Kurihara H, He RR, and Li YF (2019). Predator stress-induced depression is associated with inhibition of hippocampal neurogenesis in adult male mice. Neural Regen. Res 14, 298–305. 10.4103/1673-5374.244792. [PubMed: 30531013]
34. Barbano MF, Wang HL, Zhang S, Miranda-Barrientos J, Estrin DJ, Figueroa-González A, Liu B, Barker DJ, and Morales M (2020). VTA Glutamatergic Neurons Mediate Innate Defensive Behaviors. Neuron 107, 368–382.e8. 10.1016/j.neuron.2020.04.024. [PubMed: 32442399]

35. Rosen JB, Asok A, and Chakraborty T (2015). The smell of fear: innate threat of 2,5-dihydro-2,4,5-trimethylthiazoline, a single molecule component of a predator odor. Front. Neurosci 9, 292. 10.3389/fnins.2015.00292. [PubMed: 26379483]
36. Kalandakanond-Thongsong S, Daendee S, Thongsong B, and Chavananikul V (2010). The Efficacy of Pure Natural Repellents on Rat Responses Using Circular Open Field. Thai J. Vet. Med 40, 411–418. 10.56808/2985-1130.2259.
37. Janitzky K, D'Hanis W, Kröber A, and Schwegler H (2015). TMT predator odor activated neural circuit in C57BL/6J mice indicates TMT-stress as a suitable model for uncontrollable intense stress. Brain Res. 1599, 1–8. 10.1016/j.brainres.2014.12.030. [PubMed: 25532494]
38. Butler RK, Sharko AC, Oliver EM, Brito-Vargas P, Kaigler KF, Fadel JR, and Wilson MA (2011). Activation of phenotypically-distinct neuronal subpopulations of the rat amygdala following exposure to predator odor. Neuroscience 175, 133–144. 10.1016/j.neuro-science.2010.12.001. [PubMed: 21146592]
39. Douton JE, Norgren R, and Grigson PS (2021). Effects of a glucagon-like peptide-1 analog on appetitive and consummatory behavior for rewarding and aversive gustatory stimuli in rats. Physiol. Behav 229, 113279. 10.1016/j.physbeh.2020.113279. [PubMed: 33285178]
40. Yu JX, Xiang Q, Qu JB, Hui YM, Lin T, Zeng XN, and Liu JL (2022). Octopaminergic neurons function in appetitive but not aversive olfactory learning and memory in Bactrocera dorsalis. Insect Sci. 29, 1747–1760. 10.1111/1744-7917.13023. [PubMed: 35189034]
41. Gil-Lievana E, Ramírez-Mejía G, Urrego-Morales O, Luis-Islas J, Gutierrez R, and Bermúdez-Rattoni F (2022). Photostimulation of Ventral Tegmental Area-Insular Cortex Dopaminergic Inputs Enhances the Salience to Consolidate Aversive Taste Recognition Memory via D1-Like Receptors. Front. Cell. Neurosci 16, 823220. 10.3389/fncel.2022.823220. [PubMed: 35360496]
42. Crouse RB, Kim K, Batchelor HM, Girardi EM, Kamaletdinova R, Chan J, Rajebhosale P, Pittenger ST, Role LW, Talmage DA, et al. (2020). Acetylcholine is released in the basolateral amygdala in response to predictors of reward and enhances the learning of cue-reward contingency. Elife 9, e57335. 10.7554/eLife.57335. [PubMed: 32945260]
43. Borden PM, Zhang P, Shivange AV, Marvin JS, Cichon J, Dan C, Podgorski K, Figueiredo A, Novak O, Tanimoto M, et al. (2020). A Fast Genetically Encoded Fluorescent Sensor for Faithful in Vivo Acetylcholine Detection in Mice, Fish, Worms and Flies. Preprint at bioRxiv. 10.1101/2020.02.07.939504.
44. Teles-Grilo Ruivo LM, Baker KL, Conway MW, Kinsley PJ, Gilmour G, Phillips KG, Isaac JTR, Lowry JP, and Mellor JR (2017). Coordinated Acetylcholine Release in Prefrontal Cortex and Hippocampus Is Associated with Arousal and Reward on Distinct Timescales. Cell Rep. 18, 905–917. 10.1016/j.celrep.2016.12.085. [PubMed: 28122241]
45. Hebb ALO, Zacharko RM, Gauthier M, Trudel F, Laforest S, and Drolet G (2004). Brief exposure to predator odor and resultant anxiety enhances mesocorticolimbic activity and enkephalin expression in CD-1 mice. Eur. J. Neurosci 20, 2415–2429. 10.1111/j.1460-9568.2004.03704.x. [PubMed: 15525282]
46. Jiang L, Kundu S, Lederman JD, López-Hernández GY, Ballinger EC, Wang S, Talmage DA, and Role LW (2016). Cholinergic Signaling Controls Conditioned Fear Behaviors and Enhances Plasticity of Cortical-Amygdala Circuits. Neuron 90, 1057–1070. 10.1016/j.neuron.2016.04.028. [PubMed: 27161525]
47. Crimmins BE, Lingawi NW, Chieng BC, Leung BK, Maren S, and Laurent V (2023). Basal forebrain cholinergic signaling in the basolateral amygdala promotes strength and durability of fear memories. Neuropsychopharmacology 48, 605–614. 10.1038/s41386-022-01427-w. [PubMed: 36056107]
48. Knox D (2016). The role of basal forebrain cholinergic neurons in fear and extinction memory. Neurobiol. Learn. Mem 133, 39–52. 10.1016/j.nlm.2016.06.001. [PubMed: 27264248]
49. Mineur YS, and Picciotto MR (2021). The role of acetylcholine in negative encoding bias: Too much of a good thing? Eur. J. Neurosci 53, 114–125. 10.1111/ejn.14641. [PubMed: 31821620]
50. Eck SR, Xu SJ, Telenson A, Duggan MR, Cole R, Wicks B, Bergmann J, Lefebo H, Shore M, Shepard KA, et al. (2020). Stress Regulation of Sustained Attention and the Cholinergic Attention System. Biol. Psychiatry 88, 566–575. 10.1016/j.biopsych.2020.04.013. [PubMed: 32600739]

51. Ren LY, Cicvaric A, Zhang H, Meyer MA, Guedea AL, Gao P, Petrovic Z, Sun X, Lin Y, and Radulovic J (2022). Stress-induced changes of the cholinergic circuitry promote retrieval-based generalization of aversive memories. Mol. Psychiatry 27, 3795–3805. 10.1038/s41380-022-01610-x. [PubMed: 35551246]
52. Aitta-Aho T, Hay YA, Phillips BU, Saksida LM, Bussey TJ, Paulsen O, and Apergis-Schoute J (2018). Basal Forebrain and Brainstem Cholinergic Neurons Differentially Impact Amygdala Circuits and Learning-Related Behavior. Curr. Biol 28, 2557–2569.e4. 10.1016/j.cub.2018.06.064. [PubMed: 30100338]
53. Ananth MR, Rajebhosale P, Kim R, Talmage DA, and Role LW (2023). Basal forebrain cholinergic signalling: development, connectivity and roles in cognition. Nat. Rev. Neurosci 24, 233–251. 10.1038/s41583-023-00677-x. [PubMed: 36823458]
54. Zhu G, Du L, Jin L, and Offenhäusser A (2016). Effects of Morphology Constraint on Electrophysiological Properties of Cortical Neurons. Sci. Rep 6, 23086. 10.1038/srep23086. [PubMed: 27052791]
55. Peng H, Xie P, Liu L, Kuang X, Wang Y, Qu L, Gong H, Jiang S, Li A, Ruan Z, et al. (2021). Morphological diversity of single neurons in molecularly defined cell types. Nature 598, 174–181. 10.1038/s41586-021-03941-1. [PubMed: 34616072]
56. Udvary D, Harth P, Macke JH, Hege H-C, de Kock CPJ, Sakmann B, and Oberlaender M (2022). The impact of neuron morphology on cortical network architecture. Cell Rep. 39, 110677. 10.1016/j.celrep.2022.110677. [PubMed: 35417720]
57. Ciganok-Hückels N, Jehasse K, Kricsfalussy-Hrabár L, Ritter M, Rüland T, and Kampa BM (2023). Postnatal development of electrophysiological and morphological properties in layer 2/3 and layer 5 pyramidal neurons in the mouse primary visual cortex. Cereb. Cortex 33, 5875–5884. 10.1093/cercor/bhac467. [PubMed: 36453454]
58. Palmer D, Cayton CA, Scott A, Lin I, Newell B, Paulson A, Weberg M, and Richard JM (2024). Ventral pallidum neurons projecting to the ventral tegmental area reinforce but do not invigorate reward-seeking behavior. Cell Rep. 43, 113669. 10.1016/j.celrep.2023.113669. [PubMed: 38194343]
59. Scott A, Palmer D, Newell B, Lin I, Cayton CA, Paulson A, Remde P, and Richard JM (2023). Ventral Pallidal GABAergic Neuron Calcium Activity Encodes Cue-Driven Reward Seeking and Persists in the Absence of Reward Delivery. J. Neurosci 43, 5191–5203. 10.1523/jneurosci.0013-23.2023. [PubMed: 37339880]
60. Wulff AB, Tooley J, Marconi LJ, and Creed MC (2019). Ventral pallidal modulation of aversion processing. Brain Res. 1713, 62–69. 10.1016/j.brainres.2018.10.010. [PubMed: 30300634]
61. Saunders A, Granger AJ, and Sabatini BL (2015). Corelease of acetylcholine and GABA from cholinergic forebrain neurons. Elife 4, e06412. 10.7554/eLife.06412. [PubMed: 25723967]
62. Tooley J, Marconi L, Alipio JB, Matikainen-Ankney B, Georgiou P, Kravitz AV, and Creed MC (2018). Glutamatergic Ventral Pallidal Neurons Modulate Activity of the Habenula-Tegmental Circuitry and Constrain Reward Seeking. Biol. Psychiatry 83, 1012–1023. 10.1016/j.biopsych.2018.01.003. [PubMed: 29452828]
63. Nickerson Poulin A, Guerci A, El Mestikawy S, and Semba K (2006). Vesicular glutamate transporter 3 immunoreactivity is present in cholinergic basal forebrain neurons projecting to the basolateral amygdala in rat. J. Comp. Neurol 498, 690–711. 10.1002/cne.21081. [PubMed: 16917846]
64. Barabás B, Reéb Z, Papp OI, and Hájos N (2023). Functionally linked amygdala and prefrontal cortical regions are innervated by both single and double projecting cholinergic neurons. Preprint at bioRxiv. 10.1101/2023.12.29.573623.
65. Allaway KC, Muñoz W, Tremblay R, Sherer M, Herron J, Rudy B, Machold R, and Fishell G (2020). Cellular birthdate predicts laminar and regional cholinergic projection topography in the forebrain. Elife 9, e63249. 10.7554/eLife.63249. [PubMed: 33355093]
66. Wilson MA, and Fadel JR (2017). Cholinergic regulation of fear learning and extinction. J. Neurosci. Res 95, 836–852. 10.1002/jnr.23840. [PubMed: 27704595]

67. Paul S, Jeon WK, Bizon JL, and Han JS (2015). Interaction of basal forebrain cholinergic neurons with the glucocorticoid system in stress regulation and cognitive impairment. Front. Aging Neurosci 7, 43. 10.3389/fnagi.2015.00043. [PubMed: 25883567]

68. Mineur YS, Mose TN, Vanopdenbosch L, Etherington IM, Ogbejesi C, Islam A, Pineda CM, Crouse RB, Zhou W, Thompson DC, et al. (2022). Hippocampal acetylcholine modulates stress-related behaviors independent of specific cholinergic inputs. Mol. Psychiatry 27, 1829–1838. 10.1038/s41380-021-01404-7. [PubMed: 34997190]

69. Mei L, Zhou Y, Sun Y, Liu H, Zhang D, Liu P, and Shu H (2020). Acetylcholine Muscarinic Receptors in Ventral Hippocampus Modulate Stress-Induced Anxiety-Like Behaviors in Mice. Front. Mol. Neurosci 13, 598811. 10.3389/fnmol.2020.598811. [PubMed: 33384583]

70. Qiu Q, Wu Y, Ma L, Xu W, Hills M Jr., Ramalingam V, and Yu CR (2021). Acquisition of innate odor preference depends on spontaneous and experiential activities during critical period. Elife 10, e60546. 10.7554/eLife.60546. [PubMed: 33769278]

71. Qiu Q, Wu Y, Ma L, and Yu CR (2021). Encoding innately recognized odors via a generalized population code. Curr. Biol 31, 1813–1825.e4. 10.1016/j.cub.2021.01.094. [PubMed: 33651991]

72. Chen TW, Wardill TJ, Sun Y, Pulver SR, Renninger SL, Baohan A,Schreiter ER, Kerr RA,Orger MB,Jayaraman V,et al. .(2013). Ultrasensitive fluorescent proteins for imaging neuronal activity. Nature 499, 295–300. 10.1038/nature12354. [PubMed: 23868258]

73. Krashes MJ, Koda S, Ye C, Rogan SC, Adams AC, Cusher DS, Maratos-Flier E, Roth BL, and Lowell BB (2011). Rapid, reversible activation of AgRP neurons drives feeding behavior in mice. J. Clin. Invest 121, 1424–1428. 10.1172/jci46229. [PubMed: 21364278]

74. Grybko MJ, Hahm ET, Perrine W, Parnes JA, Chick WS, Sharma G, Finger TE, and Vijayaraghavan S (2011).A transgenic mouse model reveals fast nicotinic transmission in hippocampal pyramidal neurons. Eur. J. Neurosci 33, 1786–1798. 10.1111/j.1460-9568.2011.07671.x. [PubMed: 21501254]

75. López-Hernández GY, Ananth M, Jiang L, Ballinger EC, Talmage DA, and Role LW (2017). Electrophysiological properties of basal forebrain cholinergic neurons identified by genetic and optogenetic tagging. J. Neurochem 142, 103–110. 10.1111/jnc.14073.

76. Lara Aparicio SY, Laureani Fierro Å.d.J., Aranda Abreu GE, Toledo Cárdenas R, García Hernández LI, Coria Åvila GA, Rojas Durán F., Aguilar MEH, Manzo Denes J, Chi-Castarñeda LD, and Pérez Estudillo CA. (2022). Current Opinion on the Use of c-Fos in Neuroscience. NeuroSci 3, 687–702.

77. Barth AL, Gerkin RC, and Dean KL (2004). Alteration of neuronal firing properties after in vivo experience in a FosGFP transgenic mouse. J. Neurosci 24, 6466–6475. 10.1523/jneurosci.4737-03.2004. [PubMed: 15269256]

78. Kim Y, Venkataraju KU, Pradhan K, Mende C, Taranda J, Turaga SC, Arganda-Carreras I, Ng L, Hawrylycz MJ, Rockland KS, et al. (2015). Mapping Social Behavior-Induced Brain Activation at Cellular Resolution in the Mouse. Cell Rep. 10, 292–305. 10.1016/j.celrep.2014.12.014. [PubMed: 25558063]

79. Ting JT, Lee BR, Chong P, Soler-Llavina G, Cobbs C, Koch C, Zeng H, and Lein E (2018). Preparation of Acute Brain Slices Using an Optimized N-Methyl-D-glucamine Protective Recovery Method. J. Vis. Exp 132, 53825. 10.3791/53825.

Highlights

- VP cholinergic projection neurons are engaged in approach and avoidance behaviors
- Opposing valence odors activate distinct subpopulations of VP cholinergic neurons
- These two subpopulations differentially integrate into VP circuits
- VP cholinergic signaling is required for approach behavior

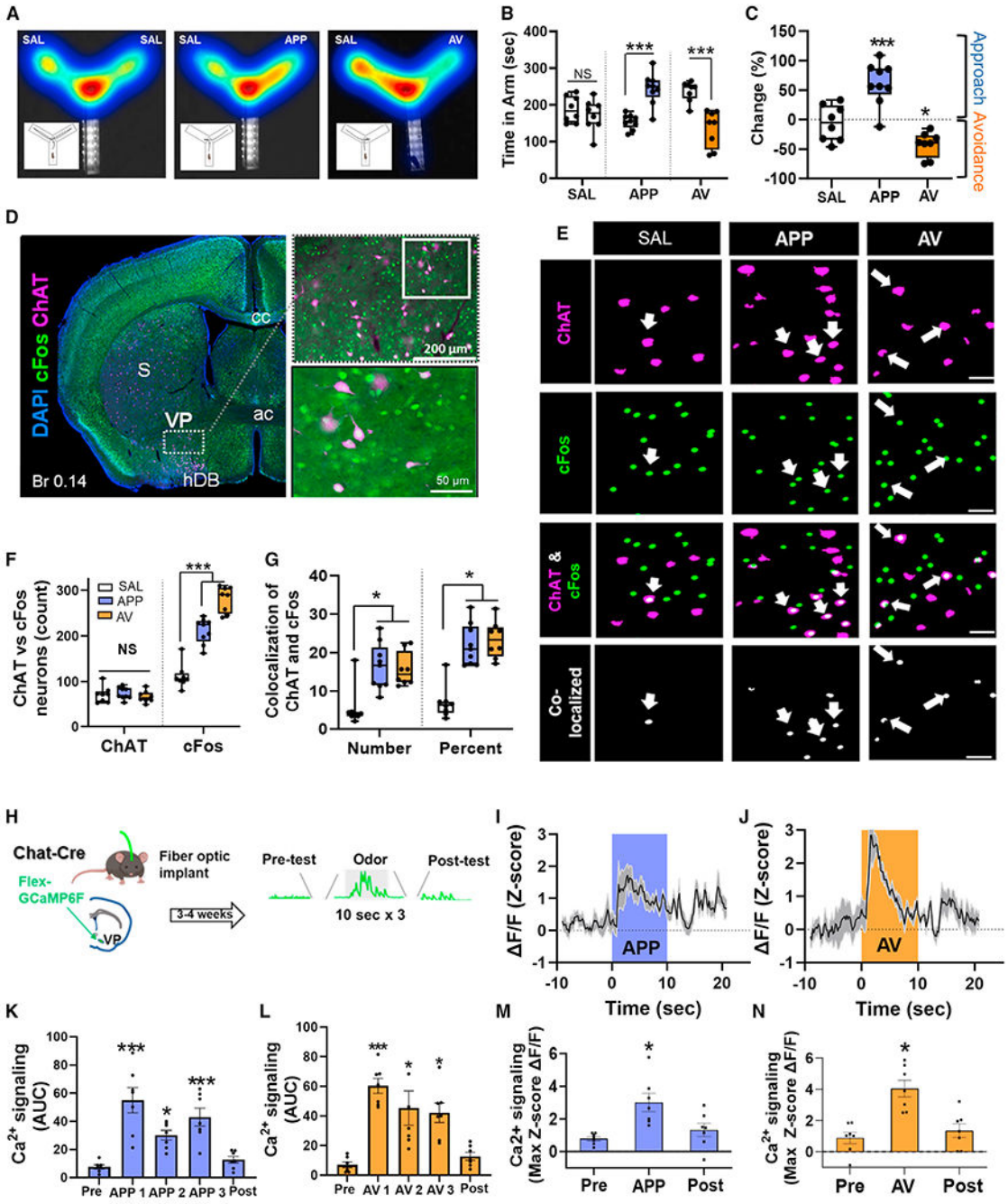

Figure 1. Appetitive and aversive odors activate VP cholinergic neurons

(A) Example heatmaps from the behavioral paradigms tested (from left to right): saline (SAL), appetitive odor (APP), aversive odor (AV). Insets illustrate the typical path traveled by mice under each condition. Left: presentation of SAL in both test arms results in approximately equal time spent in each arm. Middle: presentation of an APP odor in one arm elicits approach behavior. Right: presentation of an AV odor elicits avoidance behavior. (B) Left: total time spent in each arm under SAL vs. SAL conditions, compared with SAL vs. APP and SAL vs. AV conditions.

(C) Behavioral responses measured as percent change of time spent in odor vs. SAL arm.
(D) Left: representative image of activated cholinergic neurons in a coronal slice (Br 0.14) following odor preference test. Right: higher-magnification images of a representative area within the VP (top; scale bar, 200 μm), with additional magnification of the demarcated area in the inset shown below (scale bar, 50 μm). Blue, DAPI; green, cFos; magenta, ChAT.
(E) Representative high-magnification images of the VP following ChAT and cFos immunohistochemistry. First column, SAL; second column, APP odor; third column, AV odor. Rows are representative images for ChAT (first row), cFos (second row), the overlay between ChAT and cFos (third row), and co-localization between ChAT and cFos (fourth row). Scale bars, 50 μm. Arrowheads represent co-localized ChAT and cFos neurons in the VP.
(F) Total counts of neurons immunostained for both ChAT and cFos.
(G) Co-localization of ChAT and cFos in the VP in total numbers (left) and percentage of $ChAT^+$ neurons that co-express cFos (right).
(H) Workflow and timeline for *in vivo* fiber photometric assays.
(I and J) VP FLEX-GCaMP6f traces in response to the first 10-s delivery of the APP odor (I) and AV odor (J). Shaded area represents the time window for odor delivery.
(K and L) Area under the curve (AUC) measurements before, during, and following each APP odor (K) or AV odor (L) delivery.
(M and N) Maximum *Z*-score $\Delta F/F$ before, during, and following APP odor (M) and AV odor (N) exposure.
*$p < 0.05$, ***$p < 0.001$, NS, not significant. Error bars represent mean ± SEM. For both behavior and IHC experiments (A–G), sample sizes are as follows: SAL, n = 8 mice, 4 males and 4 females; APP odor, n = 9 mice, 4 males and 5 females; AV odor, n = 8 mice, 4 males and 4 females. For fiber photometry experiments, n = 7 mice, 5 males and 2 females.

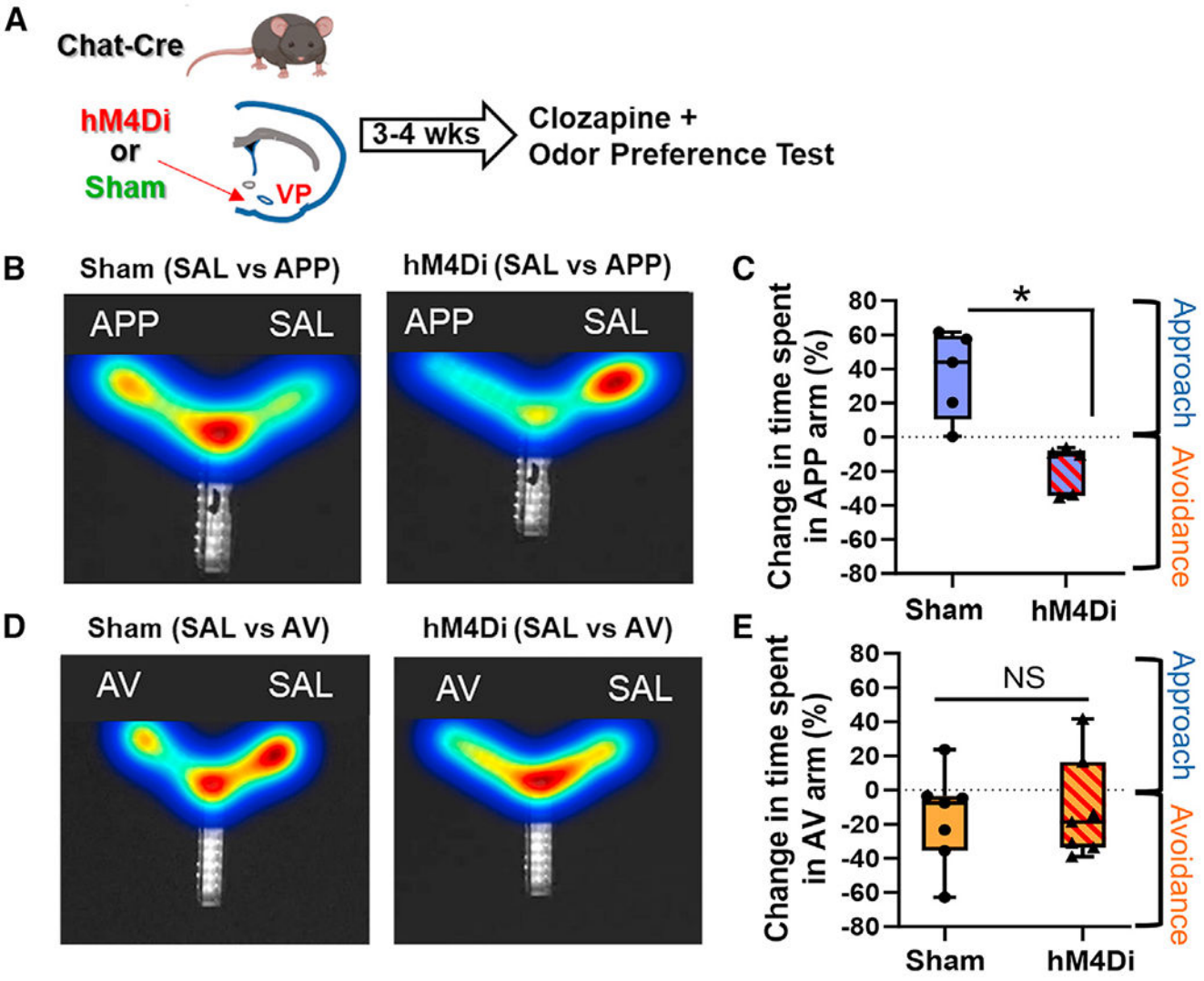

Figure 2. Chemogenetic inhibition of VP cholinergic neurons abolishes approach to the APP odor

(A) Workflow of experiments using chemogenetic inhibition to test the contribution of VP cholinergic activity to approach and avoidance behaviors in response to odor exposure.

(B) Left: representative heatmap demonstrating approach behavior to the APP odor in a sham mouse (n = 5 mice; 3 males and 2 females). Right: representative heatmap in a mouse with chemogenetic inhibition of cholinergic neurons in the VP and APP odor presentation (n = 5 mice; 2 males and 3 females).

(C) Quantification of experiments shown in (B).

(D) Left: representative heatmap demonstrating avoidance of the AV odor in a sham mouse (n = 7 mice; 5 males and 2 females). Right: representative heatmap showing that inhibition of VP cholinergic neurons (n = 7 mice; 3 females and 4 males) is without effect on avoidance of the AV odor.

(E) Quantification of experiments shown in (D).

*$p < 0.05$. Error bars represent mean ± SEM.

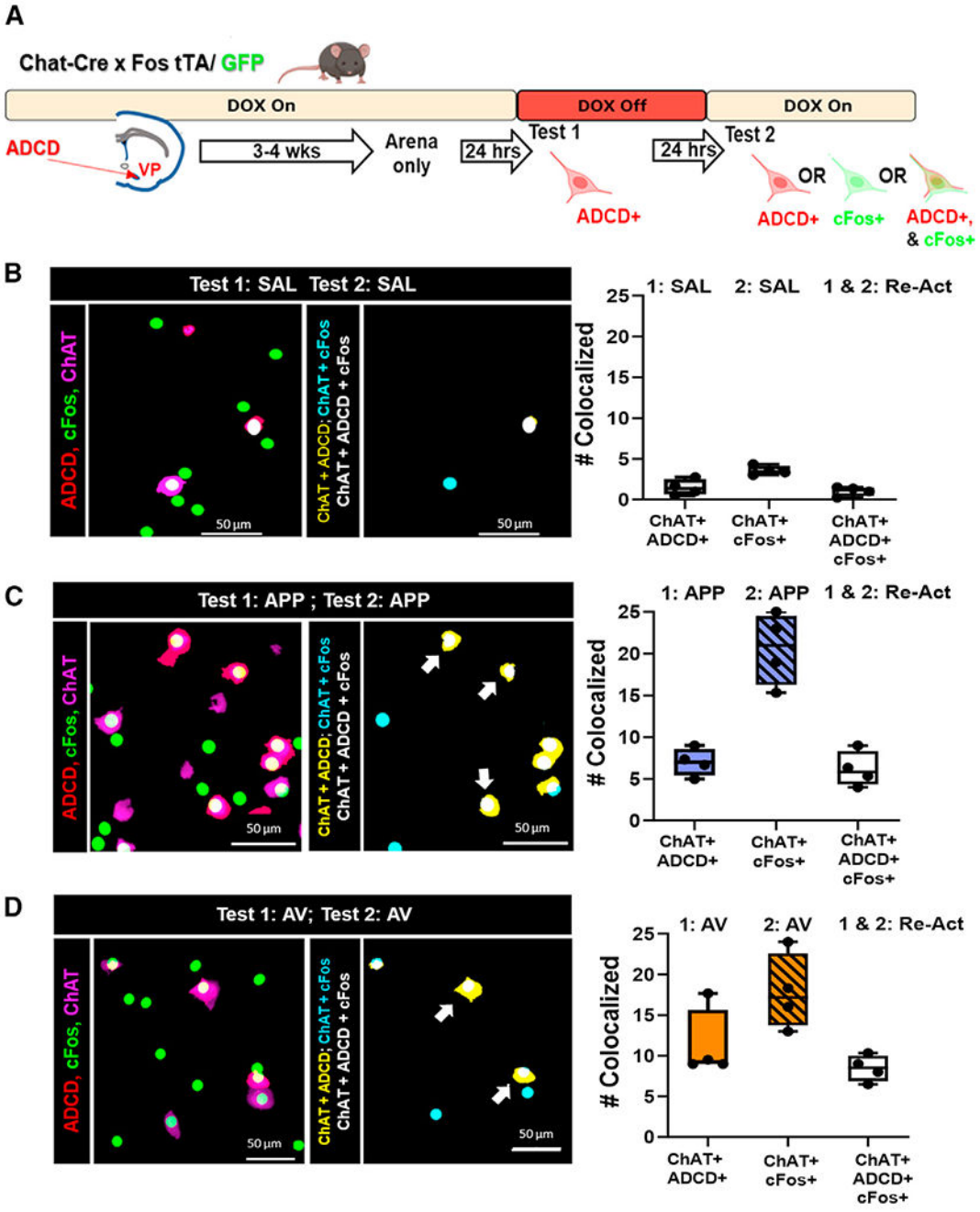

Figure 3. Assessment of activated and reactivated VP cholinergic neurons using genetic and immediate-early gene probes following repeat odor presentation

(A) Schematic diagram of the strategy employed to differentially label VP cholinergic neurons that were activated in same or distinct contexts.

(B) Mapping and quantification of the activation and reactivation profile of VP cholinergic neurons following two exposures to SAL (n = 4 mice; 2 males and 2 females). Left: representative image of ADCD (red), cFos (green), and ChAT (magenta). Mapping of the co-localization of the indicated probes is shown in the right image. Right: quantification of the number of VP cholinergic neurons activated by test 1 ($ChAT^+$ and $ADCD^+$), those

activated by test 2 (ChAT$^+$ and cFos$^+$), and the neurons that were reactivated (ChAT$^+$, ADCD$^+$, and cFos$^+$).

(C) Mapping (left) and quantification (right) of the activation and reactivation profile of VP cholinergic neurons following two test exposures to the same APP odor (n = 4 mice; 2 males and 2 females).

(D) Mapping (left) and quantification (right) of the activation and reactivation profile of VP cholinergic neurons following two test exposures to the same AV odor (n = 4 mice; 3 males and 1 female). Error bars represent mean ± SEM. Scale bars, 50 μm.

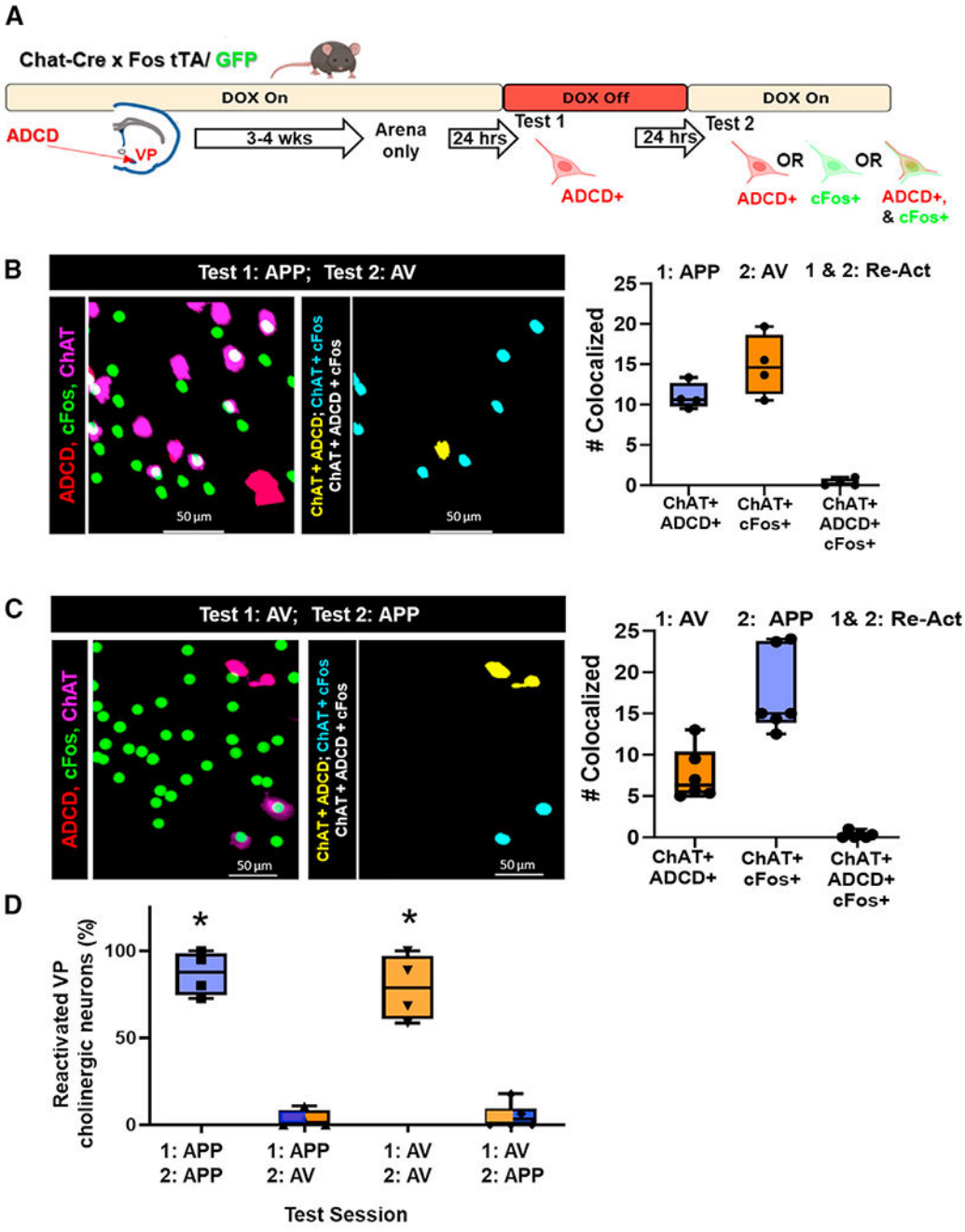

Figure 4. Distinct populations of VP cholinergic neurons are activated in response to distinct olfactory stimuli

(A) Schematic diagram of the strategy employed to label activated VP cholinergic neurons in distinct contexts (see Figure 3 legend for details).

(B) Mapping (left) and quantification (right) of the activation and reactivation profile of VP cholinergic neurons (n = 4 mice, all males) following an initial exposure to the APP odor (test 1: APP), followed 24-h later with exposure to the AV odor (test 2: AV).

(C) Mapping (left) and quantification (right) of the activation and reactivation profile of VP cholinergic neurons (n = 6 mice, all males) following an initial exposure to the AV odor (test 1: AV), followed by exposure to the APP odor (test 2: APP).

(D) Summary of the quantification of the reactivation profile of VP cholinergic neurons following two test exposures to the same odor (either APP or AV) and following exposure to opposite valence odors on test 1 vs. test 2.

*$p < 0.05$. Error bars represent mean ± SEM. Scale bars, 50 μm.

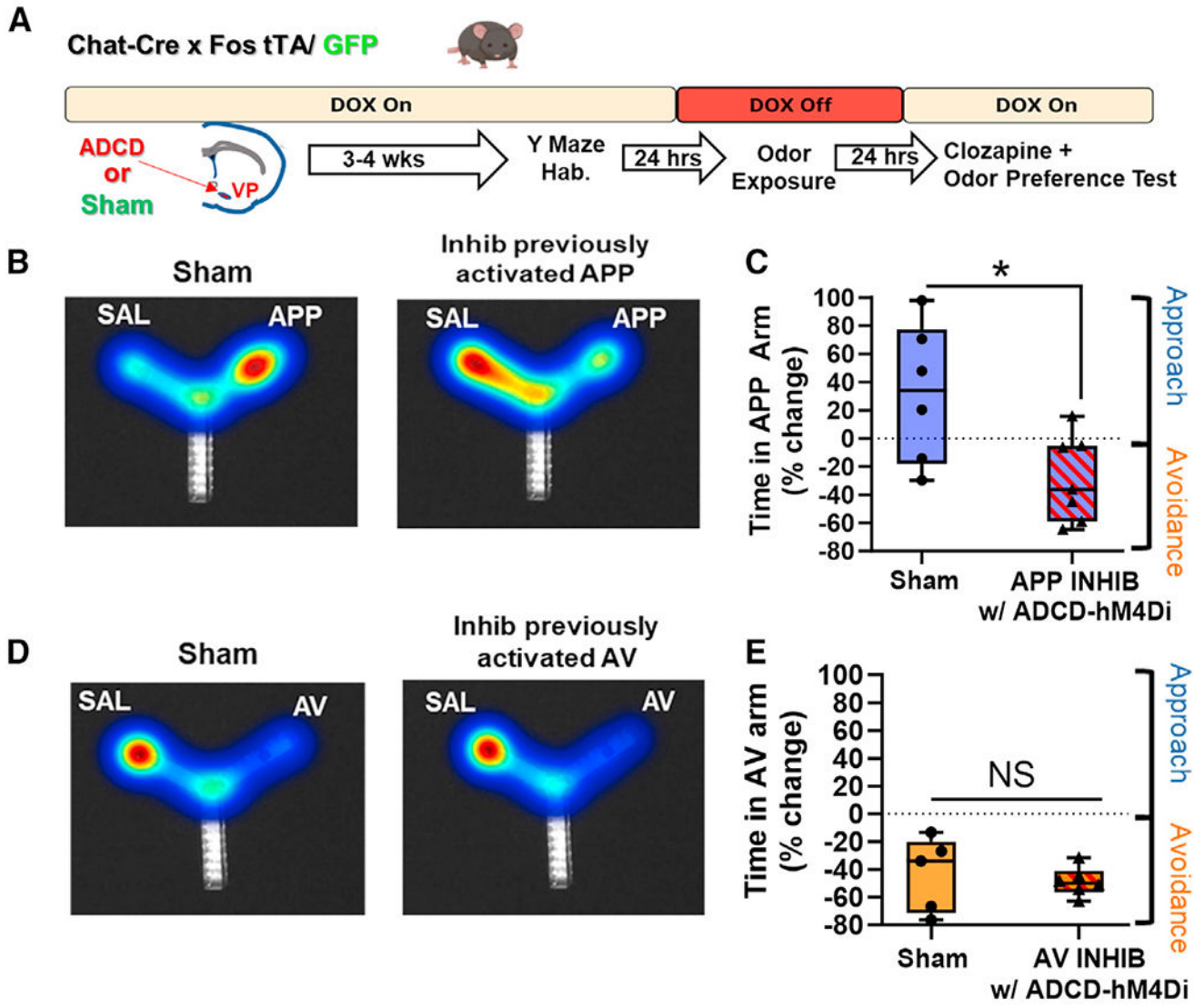

Figure 5. Selective chemogenetic inhibition of previously activated APP cholinergic neurons in the VP abolishes approach to the appetitive odor, reversing behavior to strong avoidance

(A) Workflow of behavior experiments using ADCD to target inhibitory DREADDs for specific inhibition of previously activated subpopulations of VP cholinergic neurons.

(B) Left: representative heatmap showing approach behavior to the APP odor in a sham mouse. Right: representative heatmap of the behavioral response of a mouse following inhibition of VP cholinergic neurons previously activated in response to the APP odor.

(C) Mice in the sham group (n = 6 mice; 2 males and 4 females) exhibit approach to the APP odor. Inhibiting previously activated VP cholinergic neurons in response to APP odor exposure (n = 7 mice; 5 males and 2 females) leads to significantly more time in the SAL paired arm.

(D) Left: representative heatmap depicting avoidance of the AV odor in a sham mouse (n = 5 mice). Right: ADCD inhibition of VP cholinergic neurons previously activated in response to the AV odor has no effect on avoidance of the AV odor.

(E) Mice in the sham group (n = 5; 2 males and 3 females) exhibit avoidance of the AV odor. Inhibiting VP cholinergic neurons previously activated by the AV odor (n = 6; 4 males and 2 females) has no effect.

*$p < 0.05$. Error bars represent mean ± SEM.

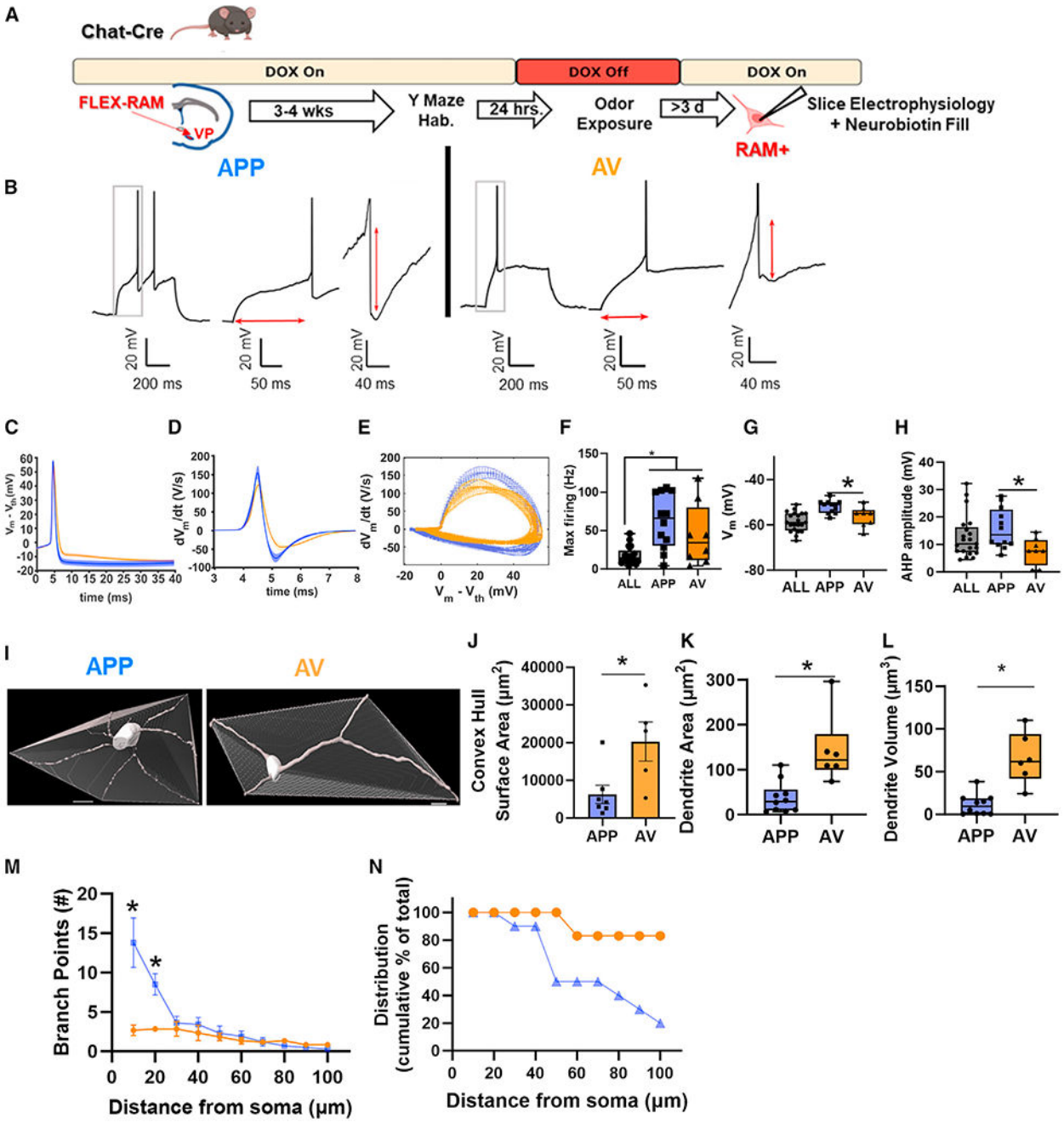

Figure 6. Differences in electrophysiological and morphological properties between appetitive vs. aversive odor activated VP cholinergic neurons

(A) Timeline of slice electrophysiology experiments using AAV.RAM.d2TTA::TRE.FLEX.tdTomato (FLEX-RAM) labeling of activated VP cholinergic neurons.

(B) Representative electrophysiology traces from an APP-odor-activated (n = 12 cells from 6 mice; 3 males and 3 females) and an AV-odor-activated VP cholinergic neuron (n = 8 cells from 4 mice; 2 males and 2 females). Left: representative traces at rheobase. Middle: traces

zoomed in to show differences in latency to fire an action potential. Right: traces zoomed in to illustrate differences in amplitude of the afterhyperpolarization potential.

(C) Extended time course of action potential currents ($V_m - V_{th}$).

(D) Action potential currents of APP vs. AV VP cholinergic neurons plotted as dV/dt vs. time.

(E) Phase plots of action potential dynamics (dV/dt vs. V) of APP vs. AV VP cholinergic neurons.

(F–H) Comparison of electrophysiological properties assayed in identified APP vs. AV VP cholinergic neurons, with VP cholinergic neurons from home-cage ChAT-tau-eGFP mice (ALL, n = 21 cells from 8 mice). APP and AV VP cholinergic neurons display differences in maximum firing rate (F), resting membrane voltage (G), and afterhyperpolarization amplitude (H).

(I) Reconstructed proximal arbor of a representative neuron from an APP (left) and AV odor VP cholinergic neuron (right), with their convex hull shown. Scale bar, 10 μm.

(J) The convex hull from APP VP cholinergic neurons (n = 7 reconstructed cells with a convex hull from 5 mice: 3 males and 2 females) are significantly smaller in surface area vs. AV VP cholinergic neurons (n = 5 reconstructed cells with a convex hull from 3 mice: 2 male and 1 female).

(K and L) APP VP cholinergic neurons (n = 10 reconstructed cells from 8 mice: 4 male and 4 female) exhibit a significantly smaller dendrite area (K) and dendrite volume (L) than AV VP cholinergic neurons (n = 6 reconstructed cells from 4 mice: 2 male and 2 female).

(M) Sholl analysis of reconstructed APP (n = 10 reconstructed cells from 8 mice: 4 male and 4 female) and AV (n = 6 reconstructed cells from 4 mice: 2 male and 2 female) VP cholinergic neurons.

(N) A larger percentage of AV VP cholinergic neurons are able to reach greater distances away from the soma vs. APP VP cholinergic neurons.

*$p < 0.05$. Symbols represent individual cells or reconstructed neurons. Error bars represent mean ± SEM.

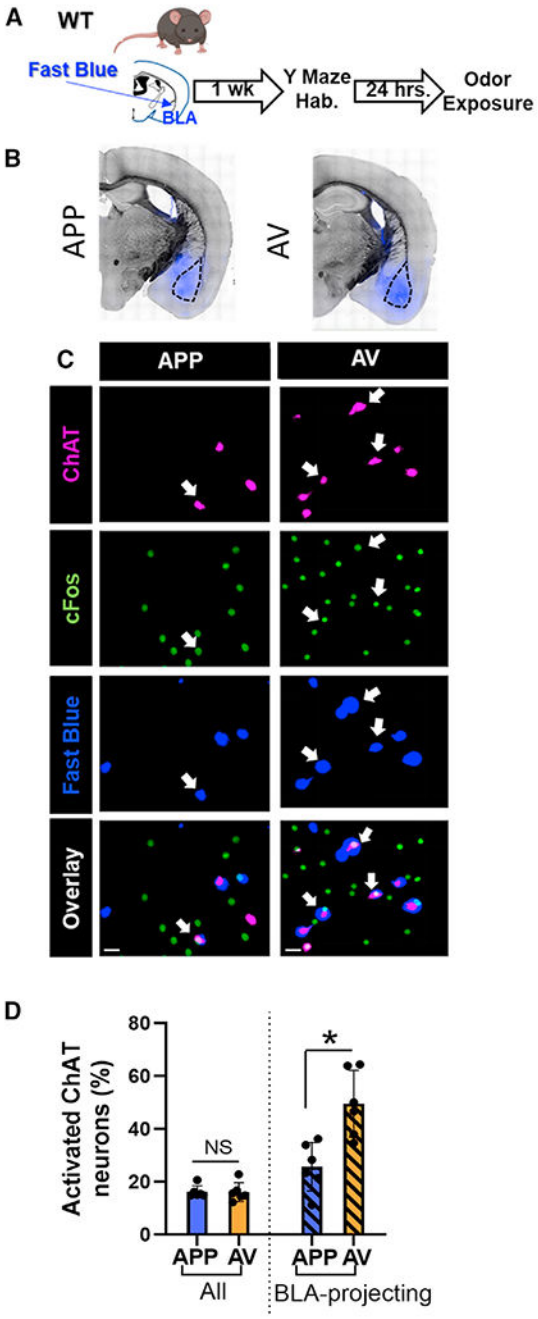

Figure 7. Although both APP and AV VP cholinergic neurons project to the BLA, the predominant BLA input from the VP stems from AV encoding VP cholinergic neurons

(A) Workflow to retrogradely label BLA-projecting VP cholinergic neurons.

(B) Representative images in mice injected with fast blue in the BLA (in blue) and overlaid on a bright-field image.

(C) Representative images from the VP in a mouse exposed to the APP odor (left column) and AV odor (right column). First row, ChAT; second row, cFos; third row, Fast Blue; bottom row, overlay of all channels. Scale bars, 20 μm.

(D) AV responsive VP cholinergic neurons (n = 6 mice, all female) constitute a significantly greater percentage of BLA-projecting VP cholinergic neurons than APP responsive VP cholinergic neurons (n = 6 mice; 4 male and 2 female).
*$p < 0.05$. Error bars represent mean ± SEM.

KEY RESOURCES TABLE

REAGENT or RESOURCE	SOURCE	IDENTIFIER
Antibodies		
Goat Anti-Choline Acetyltransferase	Millipore Sigma	Cat # AB144P; RRID: AB_2079751
Rabbit Anti-cFos	Synaptic Systems	Cat # 226 008; RRID: AB_2891278
Chicken Anti-GFP	Abcam	Cat # ab13970; RRID: AB_300798
Mouse Anti-mCherry	Living Colors	Cat # 632543; RRID: AB_2307319
Rat Anti-Substance P	Millipore Sigma	Cat # MAB356; RRID: AB_94639
Donkey Anti-Goat, Alexa Fluor 647	Thermo Fisher	Cat # A-21447; RRID: AB_2535864
Donkey Anti-Rabbit, Alexa Fluor 488	Thermo Fisher	Cat # A-21206; RRID: AB_2535792
Donkey Anti-Chicken, Alexa Fluor 488	Jackson Immuno Research	Cat # 703-545-155; RRID: AB_2340375
Donkey Anti-Mouse, Alexa Fluor 594	Thermo Fisher	Cat # A-21203; RRID: AB_141633
Donkey Anti-Rat, Alexa Fluor 594	Thermo Fisher	Cat # A-21209; RRID: AB_2535795
Streptavidin conjugated to Alexa Fluor 594	Thermo Fisher	Cat #S32356
Bacterial and virus strains		
AAV_9.DIO.TRE.hM4Di.P2A.m.Cherry (ADCD)	This paper and (Rajebhosale, Ananth et al.)[25]	N/A
AAV_9.RAM.d2tTA.TRE.mCherry.NLS-FLAG (RAM)	(Sorensen et al.)[26]	Plasmid # 63931; RRID: Addgene_63931
AAV_9.Syn.Flex-GCaMP6f.WPRE.SV40 (GCaMP6f)	(Chen et al.)[72]	Plasmid # 100837; Cat # 100837-AAV9; RRID: Addgene_100837
AAV_8.hSyn.DIO.hM4Di (Gi).mCherry (hM4Di)	(Krashes et al.)[73]	Plasmid # 44362; Cat # 44362-AAV8; RRID: Addgene_44362
AAV_9.eSyn.eGFP	Vector Biolabs	Cat # VB4870
AAV_9.RAM.d2tTA.TRE.Flex.tdTomato	(Sorensen et al.)[26]	Plasmid # 84468; RRID: Addgene_84468
Chemicals, peptides, and recombinant proteins		
Fast Blue	Polysciences	Cat # 17740-1
2-phenylethanol	Sigma	Cat # 77861
Mountain Lion Urine	Predator Pee	Cat # 92016
Peppermint Oil	Sigma	Cat # 77411
Peanut butter Oil	Commercially available	N/A
Clozapine	Sigma	Cat #C6305
Normal Donkey Serum	Jackson Immuno Research	Cat # 017-000-121
Fluoromount-G with DAPI	Southern Bio Tech	Cat # 0100-01
Neurobiotin	Vector Laboratories	Cat # SP-1120
Experimental models: Organisms/strains		
Mouse: C57BL/6J	The Jackson Laboratory	Jax Strain # 000664
Mouse: Chat-IRES-Cre:Δneo	The Jackson Laboratory	Jax Strain # 006410
Mouse: Fos-tTA/Fos-shEGFP	The Jackson Laboratory	Jax Strain # 018306
Mouse: Chat-tau-eGFP	From S.Vijayaraghavan, University of Colorado	N/A
Software and algorithms		

REAGENT or RESOURCE	SOURCE	IDENTIFIER
Custom MATLAB script for fiber photometry analysis	This paper	https://doi.org/10.5281/zenodo.10723901
Custom MATLAB script for electrophysiology analysis	This paper	https://doi.org/10.5281/zenodo.10723870
MATLAB (2020a)	Mathworks	https://www.mathworks.com/products/matlab.html RRID:SCR_001622
Imaris	Oxford Instruments	https://imaris.oxinst.com/ RRID:SCR_007370
EthoVision XT (v 15)	Noldus	https://www.noldus.com/ethovision-xt RRID:SCR_000441
Graphpad Prism (v 10)	Graphpad	https://www.graphpad.com/features RRID: SCR_002798
Sigmaplot (v 14.0)	SYSTAT	https://systatsoftware.com/sigmaplot/
Other		
Y-Maze	Med-Associates	Cat # MED-YMMN https://med-associates.com/product/modular-y-maze-package/
Fiber optic cannulae (ferrule diameter 1.25 mm, core diameter 400 μm)	Neurophotometrics	https://neurophotometrics.com/cannulae-and-sleeves
Ceramic split sleeves to connect fiber optic cannula to patch cord	Neurophotometrics	https://neurophotometrics.com/cannulae-and-sleeves
Fiber optic patch cords	Doric	https://neuro.doriclenses.com/collections/branching-fiber-optic-patchcords/products/laf-bundle-fiber-optic-patch-cord?